Journal of Structural Geology 30 (2008) 899–917

Contents lists available at ScienceDirect

Journal of Structural Geology

journal homepage: www.elsevier.com/locate/jsg

Theories and applicability of grain size piezometers: The role of dynamic recrystallization mechanisms

I. Shimizu*

Department of Earth and Planetary Science, University of Tokyo, 7-3-1 Hongo, Bunkyo-ku, Tokyo 113-0033, Japan

ARTICLE INFO

Article history:
Received 10 January 2007
Received in revised form 3 March 2008
Accepted 12 March 2008
Available online 31 March 2008

Keywords:
Dynamic recrystallization
Grain size
Stress
Dislocation creep
Quartz

ABSTRACT

The average grain size (d) arising from dynamic recrystallization (DRX) is often used as an indicator of flow stress (σ); however, a theoretical basis for the scaling relation between d and σ has yet to be well established. In this paper, theories for the development of recrystallized grain size are reviewed and their applicability is examined. Special attention is paid to the dependence of the d–σ relation on DRX mechanisms. Steady-state DRX is classified into discontinuous DRX with bulging (BLG) nucleation + grain boundary migration (GBM) and continuous DRX with subgrain rotation (SGR) nucleation + GBM. The nucleation-and-growth model derived from Derby–Ashby theory describes the former case, whereas that derived from Shimizu theory applies to the latter. A static energy-balance model derived from Twiss theory is applicable to subgrain size, but not to recrystallized grain size. The lower limit of grain size is possibly constrained by a change in deformation mechanism from dislocation creep to diffusion creep, because deformation-induced grain size reduction ceases in the diffusion creep field. Scaling relations determined in the laboratory support the Shimizu model in the case of SGR + GBM. The theoretical piezometer calibrated for quartz suggests significant temperature effects under low-temperature metamorphic conditions.

1. Introduction

Dynamic recrystallization (DRX) is considered to be one of the key mechanisms of grain size reduction in shear zones (Tullis and Yund, 1985). It has been demonstrated that during DRX the average grain size d is primarily dependent on flow stress σ and that normalised values of d and σ for various materials obey the following universal relation:

$$\frac{d}{b} = K\left(\frac{\sigma}{\mu}\right)^{-p}, \tag{1}$$

where b is the length of the Burgers vector, μ is the shear modulus, and K is a non-dimensional constant, the order of which is typically 10 (Twiss, 1977; Poirier, 1985). A similar relation, although with a different scaling factor K', is known for the subgrain size d' of various materials (Takeuchi and Argon, 1976; Twiss, 1977; Derby, 1991):

$$\frac{d'}{b} = K'\left(\frac{\sigma}{\mu}\right)^{-p'}. \tag{2}$$

The stress exponent p' of subgrain size is found to be close to unity, but p of recrystallized grain size is slightly larger than 1 in many cases, as detailed below. Empirical relations in the form of Eq. (1) are widely used to estimate paleostress in crustal shear zones (White, 1979b; Christie and Ord, 1980; Kohlstedt and Weathers, 1980; Etheridge and Wilkie, 1981; Ord and Christie, 1984; Stöckhert et al., 1999), orogenic belts (Dunlap et al., 1997; Zulauf, 2001) and the upper mantle (Mercier, 1980), because recrystallized grain size is easily measured under the optical microscope and is believed to be stable during the post-deformation history of the rock mass relative to other stress indicators such as dislocation density and subgrain size (White, 1979a; Ross et al., 1980).

The theory presented by Twiss (1977) has long been quoted as a theoretical basis for grain size piezometry. In this theory, 'stable' grain size or subgrain size is derived based on a comparison between free dislocation energy and (sub)grain boundary energy in the same volume. The Twiss theory predicts that the coefficients K and K' are temperature-independent, meaning that recrystallized grain size and subgrain size are solely dependent on flow stress; however, Twiss (1977) presented only an outline of his model, and its validity has yet to be closely scrutinized. A full description of his theory appeared in a later conference volume (Twiss, 1980), and it is this full account that is summarized in the present paper.

While the piezometer of Twiss (1977) is still used for paleostress analysis, several different models have since been proposed with

* Corresponding author. Tel.: +81 2 5841 4513; fax: +81 3 5841 45469.
E-mail address: ichiko@eps.s.u-tokyo.ac.jp

0191-8141/$ – see front matter © 2008 Elsevier Ltd. All rights reserved.
doi:10.1016/j.jsg.2008.03.004

regard to recrystallized grain size (Derby and Ashby, 1987; Derby, 1990, 1991; De Bresser et al., 1998; Shimizu, 1998b; Austin and Evans, 2007) because the static model of Twiss (1977, 1980) is inconsistent with the continuously changing nature of microstructures observed in DRX (Poirier, 1985; Shimizu, 1998b). In this regard, De Bresser et al. (2001) compiled and compared theoretical predictions and experimental results in existing literature; however, the limitations and applicability of different theories have not been fully discussed. The results of recent experimental studies suggest that the stress dependence of grain size may be different for different mechanisms of DRX (Rutter, 1995; Stipp and Tullis, 2003); this point should be taken into account in the calibration of piezometric relations.

The aim of the present paper is to clarify the predictions and limitations of existing theories of recrystallized grain size, and re-examine empirical piezometric relations taking into account the deformation conditions, recrystallization mechanisms, and time-evolution of grain size distribution in DRX.

2. Classification of dynamic recrystallization

DRX is characterized by the reconstruction and rearrangement of grain boundaries during plastic deformation at elevated temperatures (Poirier, 1985). The concept of DRX was first established in metallurgy and subsequently introduced to the study of Earth materials. Although the processes of DRX are basically the same for metals and non-metals such as rock-forming minerals, the detailed mechanisms of recrystallization and microstructural features vary among different materials and deformation conditions. This has led to some confusion in classifications of DRX and interpretations of piezometric relations, as discussed below. Here, we briefly review the terminology of DRX.

DRX was originally proposed for fcc metals such as Cu, Ni, and γ-Fe (Sellars, 1978), in which recovery processes are relatively slow. DRX was proposed as an alternative mechanism of recovering dense accumulations of dislocations, and the process of DRX was described as follows (Sakai, 1989; Humphreys and Hatherly, 1995). When materials are strained to certain critical values, nucleation occurs at the margins of existing grains by local grain boundary bulging (BLG). At this stage, the material is characterized by a 'necklace' structure (Sakai and Jonas, 1984), whereby nuclei grow at the expense of existing grains. This stage is characterized by strain softening that arises from grain boundary migration (GBM) driven by differences in dislocation energy: highly deformed older grains (i.e., hard grains) are replaced by relatively undeformed grains via the migration of grain boundaries. With increasing strain, the recrystallized grains themselves are deformed, leading to a progressive increase in dislocation density. Nucleation then occurs at the margins of these grains, and the process described above is repeated. Cyclic events of nucleation-and-growth can lead to oscillations in flow stress within stress–strain curves (Luton and Sellars, 1969; Sakai and Jonas, 1984).

Aside from the classical view of DRX described above, a mechanism of strain-induced polygonization resulting from the progressive misorientation of subgrains, termed 'recrystallization *in situ*' by Sellars (1978), has been recognized in some metals, although this process was initially regarded as a recovery process rather than DRX. Microstructures indicative of subgrain rotation (SGR) are commonly observed in minerals such as quartz (e.g., Hobbs, 1968), olivine (Poirier and Nicolas, 1975), calcite (Schmid et al., 1980), and halite (Guillopé and Poirier, 1979) that have undergone syn-tectonic deformation or high-temperature creep in the laboratory. Poirier (1985) extended the concept of DRX to include 'recrystallization *in situ*', and classified its mechanisms into two categories: DRX that proceeds by the progressive lattice misorientation of subgrains without considerable grain growth, defined as 'rotation recrystallization', and DRX accompanied by extensive GBM, defined as 'migration recrystallization'. Recrystallization initiated by SGR is also currently recognized as a common DRX mechanism in the hot-working of metals, and is referred to as 'continuous DRX' in metallurgy; DRX in the original sense is referred to as 'discontinuous DRX' (e.g., Gottstein and Mecking, 1985; Drury and Urai, 1990; Humphreys and Hatherly, 1995). Previously, dynamic recovery and DRX were regarded as mutually exclusive and competing processes (Sellars, 1978; Toriumi, 1982; Twiss and Sellars, 1978; Yund and Tullis, 1991); however, this view is only applicable to discontinuous DRX: in continuous DRX, dynamic recovery acts to enhance SGR and thereby DRX.

The classification of DRX into 'migration' and 'rotation' types, or 'GBM' and 'SGR' recrystallization (Mercier, 1980; Avé Lallemant, 1985), has been widely used in the geologic literature; however, observations by optical microscope and transmission electron microscope (TEM) of deformed quartz from ductile shear zones indicate that SGR and GBM can occur sequentially during DRX (White, 1973). The occurrence of the formation of new grains by SGR followed by GBM has also been confirmed in 'see-through' deformation experiments using sodium nitrate ($NaNO_3$) (Tungatt and Humphreys, 1981). Because the occurrence of SGR does not necessarily indicate the absence of GBM, the classification of DRX into 'migration' and 'rotation' is misleading and inadequate (Shimizu, 1998b). Following the same line of reasoning, Drury and Urai (1990) proposed three end-member mechanisms: 'SGR', 'GBM', and 'general' recrystallization. In considering deformation and recrystallization in quartzites, Hirth and Tullis (1992) defined three characteristic regimes; Stipp et al. (2002a,b) classified DRX of quartz in nature and experiments into 'BLG', 'SGR', and 'GBM' recrystallization. These categories are also applied to DRX in other minerals (Passtier and Trouw, 2005).

In the present paper, DRX is described in terms of nucleation-and-growth because BLG and SGR are mechanisms of nucleation, whereas GBM is a process that leads to grain growth. The mechanisms of discontinuous DRX (DDRX) and continuous DRX (CDRX), from their beginning to steady states, are summarized in Fig. 1. Each of the fundamental processes involved in DRX are further discussed in the following section.

3. Recrystallization mechanisms

3.1. Grain boundary migration and grain growth

In single-phase materials of uniform chemical composition, surface energy (or grain boundary energy) E_{surf} and strain energy (mainly dislocation energy) E_{strain} are possible driving forces of grain growth. In static grain growth driven by surface energy, larger grains are energetically favorable, and continue to grow at the expense of smaller grains (Hillert, 1965). Conversely, in DRX, newly recrystallized small grains (nuclei) tend to grow at the expense of

recrystallization process		transient → steady	
Discontinuous DRX	nucleation	BLG	
	grain growth	*none*	GBM
Continuous DRX	nucleation	SGR	
	grain growth	*none*	GBM

Fig. 1. Classification of DRX processes and recrystallization mechanisms from transient to steady states. BLG: bulge nucleation; SGR: nucleation by subgrain rotation; GBM: grain boundary migration.

larger grains to reduce the strain energy of the material. The growth of nuclei is enabled when the strain energy of the deformed matrix is sufficiently large to overcome surface-energy-driven shrinkage of the nuclei; i.e., when $E_{strain} > E_{surf}$. Neglecting the secondary contribution of E_{surf}, the driving force F of grain growth by strain-induced GBM is scaled as follows:

$$F \propto \sigma^{j}, \tag{3}$$

where the exponent j varies from 1 to 2 depending on the relative contributions of free dislocation energy and sub-boundary energy (Appendix A). Because the formation of a sub-boundary is an energetically favorable process (e.g., Appendix B), dislocations tend to be ordered into sub-boundaries, meaning that j is close to 1 in recovered states.

The radial grain growth rate $\dot{R}$ of a grain is described as a product of the mobility M of the grain boundary and the driving force F:

$$\dot{R} = MF. \tag{4}$$

The mobility is defined by

$$M = \frac{bwD_{gb}}{kT}, \tag{5}$$

where w is the width of the boundary, k is the Boltzmann constant, T is the absolute temperature, and D_{gb} is the diffusion coefficient at the grain boundary. D_{gb} depends on temperature as follows:

$$D_{gb} = D^{0}_{gb} \exp\left(-\frac{Q_{gb}}{RT}\right), \tag{6}$$

where D^{0}_{gb} is a constant, R is the gas constant, and Q_{gb} is the activation energy of grain boundary diffusion.

Applying Eqs. (3), (5), and (6) to Eq. (4), the growth rate is expressed as

$$\dot{R}(\sigma, T) \propto \sigma^{j} \exp\left(-\frac{Q_{gb}}{RT}\right). \tag{7}$$

Deformation-induced GBM is therefore activated at high-σ/high-T conditions, under which the effects of both F and M are large. The transition from 'rotation' to 'migration' recrystallization in halite (Guillopé and Poirier, 1979) and sodium nitrate (Tungatt and Humphreys, 1984) at elevated stress and temperature is understood by increases in F and M, respectively. In ionic crystals, the mobility of the grain boundary is sensitive to the concentrations of impurities; consequently, the impurity drag term must be added to the driving force (Poirier, 1985).

When steady-state recovery-controlled creep is achieved, the strain rate $\dot{\varepsilon}$ is written as

$$\dot{\varepsilon} = A\sigma^{n} \exp\left(-\frac{Q_{c}}{RT}\right), \tag{8}$$

where A and n are constants, and Q_c is the activation energy of dislocation creep. Eq. (7) is then modified to

$$\dot{R}(\dot{\varepsilon}, T) \propto \dot{\varepsilon}^{j/n} \exp\left(-\frac{nQ_{gb} - jQ_{c}}{nRT}\right). \tag{9}$$

Here, $\dot{\varepsilon}$ is taken as a controlling parameter instead of σ. For recovery-controlled creep in most materials, $j \simeq 1$, $n = 3$–5, and $nQ_{gb} - jQ_{c} > 0$ may be used; hence, the growth rate is expected to increase with increasing T under fixed $\dot{\varepsilon}$.

3.2. Nucleation mechanisms in dynamic recrystallization

The strain energy in minerals deformed in the crust and mantle is usually in the order of 10 J/mol (Wintsch and Dunning, 1985), which is insufficient to produce a critical nucleus by thermal fluctuation (Burrows et al., 1979; Gottstein and Mecking, 1985); therefore, BLG and SGR have been considered as nucleation mechanisms in DRX (Fig. 2). In the cases of BLG and SGR, nuclei larger than the critical size are formed in highly strained parts of the matrix.

In BLG nucleation (Fig. 2a), a section of a grain boundary pinned by impurities (Bailey and Hirsch, 1962) or sub-boundaries (Richardson et al., 1966) locally bows out due to strain-induced boundary migration; the dislocation-free region produced behind the migrating boundary then becomes a nuclei. Grain boundary bulging is basically a process of GBM; however, in the present paper the term 'GBM' is used to describe a grain-coarsening mechanism and 'BLG' to describe a mechanism that generates serrated grain boundaries, thereby resulting in nucleation. In other words, GBM is used for the migration of a grain boundary as a whole, leading to grain growth (and reduction in the size of neighboring grains), whereas BLG refers to the local migration of a grain boundary that yields a potential nucleation site; admittedly, it might be difficult to distinguish between these two cases in actual materials. For subsequent nucleation to occur, it is necessary to form a new boundary that separates the strain-free bulge from the host grain (Bellier and Doherty, 1977; Urai et al., 1986); in fact, rotation of the bulge with respect to the host grain is necessary in this regard. Grain boundary nucleation by BLG was originally proposed for fcc metals; however, evidence of BLG has also been reported from rock-forming minerals such as quartz (Hirth and Tullis, 1992), feldspar (Post and Tullis, 1999), and calcite (Pieri et al., 2001; Ter Heege et al., 2002). These findings indicate that nucleation mechanisms are not unique to

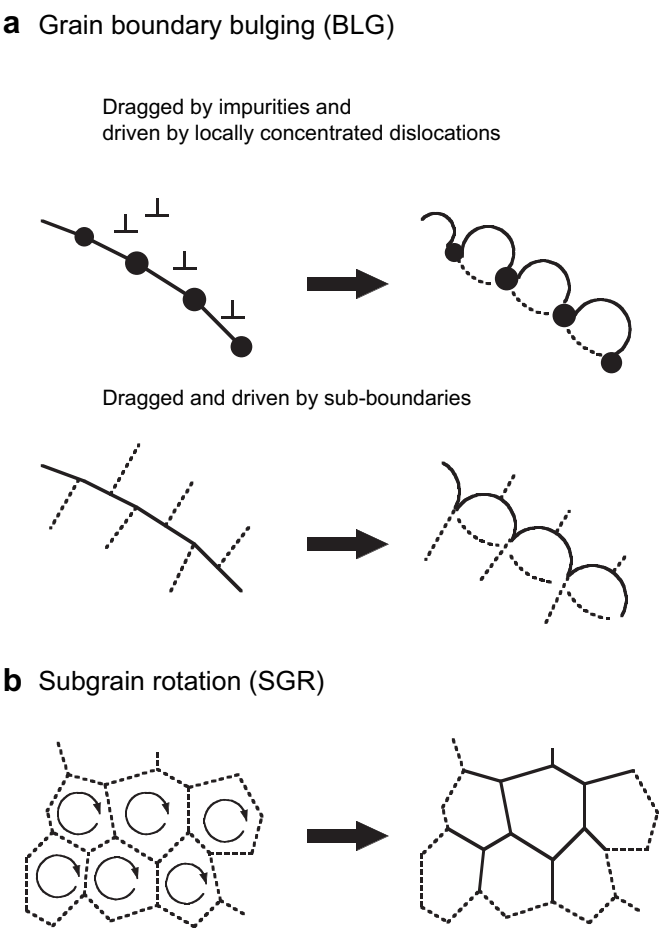

Fig. 2. Nucleation processes in DRX. See text for explanation.

individual materials and that different mechanisms may be active within a given material under different deformation conditions.

In SGR nucleation (Fig. 2b), a high-angle boundary forms via progressive lattice misorientation between subgrains. The critical angle θ_c used to differentiate low- and high-angle boundaries is conventionally taken to be 10–15° (Humphreys and Hatherly, 1995). SGR has been observed not only in minerals but also in metals such as Al and Mg-alloys (e.g., Drury et al., 1985). Nucleation by BLG is restricted to grain boundary sites, whereas both intracrystalline and marginal nucleation occur in SGR (Fig. 3) In deformation experiments of calcite using a gas-medium apparatus, Schmid et al. (1980) demonstrated that the sites of SGR nucleation change with applied stress. At high stress (20–100 MPa), equiaxed subgrains and new grains are localized around pre-existing grain boundaries and show a core-and-mantle structure. At lower stress (up to 20 MPa), however, subgrains and newly crystallized grains penetrate the entire domain of old grains.

3.3. Change in recrystallization mechanisms with deformation conditions

This section considers how DRX mechanisms change with deformation conditions. Quartz is discussed as a model material, because many studies have performed extensive microstructural analysis on both field and laboratory samples. In a series of constant-strain-rate experiments on quartzite, Hirth and Tullis (1992) distinguished three dislocation creep regimes, named Regimes 1, 2, and 3 at low-T/high-$\dot{\varepsilon}$, intermediate-T/intermediate-$\dot{\varepsilon}$, and high-T/low-$\dot{\varepsilon}$ conditions, respectively (Fig. 4a). Regime 1 is characterized by intracrystalline deformation with tangled dislocations at TEM scales and strain-weakening behavior in stress–strain curves. Recrystallization occurs at original grain boundary sites by BLG. Regime 2 is characterized by flattening of the original grains and the formation of optically visible subgrains and recrystallized grains at their rims, leading to the development of core-and-mantle structure. TEM observations reveal the arrangement of dislocations into tilt boundaries. In Regime 3, recovered microstructures are similar to those in Regime 2; however, GBM becomes active and recrystallization occurs throughout the sample, resulting in a mosaic texture with complete recrystallization.

According to the scheme of Poirier (1985), Regime 2 is classed as 'rotation' recrystallization, while Regimes 1 and 3 both fall into the category of 'migration' recrystallization, although the characteristics of 'migration' in Regimes 1 and 3 are different: in Regime 1, localized migration arises from heterogeneously distributed dislocations that contribute to the driving force F in Eq. (4), whereas in Regime 3, GBM occurs because of the enhanced mobility M of grain boundaries at high temperatures. In the present scheme (Fig. 1), Regime 1 is regarded as DDRX because of the microstructural features and mechanical behaviors described above, whereas Regimes 2 and 3 are both classified as CDRX.

The transition from Regime 1 to 2 is characterized by a change in nucleation mechanism from BLG to SGR. This change is possibly induced by rapid dynamic recovery at high-T/low-$\dot{\varepsilon}$ conditions, resulting in a decrease in free dislocation density ρ, which in turn reflects flow stress σ, as indicated by Eq. (A.5) in Appendix A. Hence, σ might be considered as a controlling parameter of the Regime 1–2 transition. The transition from BLG in Regime 1 to marginal SGR in Regime 2 is gradual rather than abrupt. In addition to BLG, Hirth and Tullis (1992) recognized a mechanism of marginal nucleation by the misorientation of very small ($<$0.1 μm) dislocation cells in Regime 1. BLG nucleation itself involves a rotational component, as mentioned in Section 3.2. Stipp and Kunze (2008) described the lattice misorientation of grain boundary bulges in Regime 1 samples. In practice, it is difficult to clearly distinguish BLG followed by lattice misorientation from marginal SGR that leads to grain boundary serration.

The transition from Regime 2 to 3 has been explained in terms of increased migration velocity (Hirth and Tullis, 1992; Hirth et al., 2001); however, the velocity of GBM in Eq. (9) is expected to increase toward high-T/high-$\dot{\varepsilon}$ conditions rather than high-T/low-$\dot{\varepsilon}$ conditions. To explain the boundary between Regimes 2 and 3, it is necessary to take into account the time-evolution of recrystallized microstructures. It should be noted that SGR is a nucleation mechanism in DRX, not a steady-state dislocation creep mechanism in itself; hence, Regime 2 is not a final state, but is considered as a transient state before the onset of grain growth. The change in DRX mechanism from 'rotation' to 'migration' with increasing strain has been observed in deformation experiments of NaCl (Poirier, 1985) and marble (Rutter, 1995). It is possible that GBM in quartz appears to be active at low-$\dot{\varepsilon}$ conditions because of the longer durations of low-$\dot{\varepsilon}$ experiments: the time taken to reach a given strain at a given temperature is longer for low-$\dot{\varepsilon}$ runs.

3.4. Microstructural evolution from transient to steady states

The microstructural descriptions provided by Hirth and Tullis (1992) were mainly based on experiments on quartzite with a mean grain size of 100–200 μm. If the initial grain size in these experiments had been smaller, recrystallization would have attained completion in a shorter time and at a smaller strain. Recrystallization microstructures are therefore not only dependent on the state variables of T and $\dot{\varepsilon}$ (or σ), but also on total strain ε, the duration of deformation, and the initial grain size d_i (Sakai and Jonas, 1984; Sakai, 1989; Ulrich et al., 2006). If d_i is smaller than the steady-state grain size, grain coarsening occurs rather than grain size reduction. In the deformation experiments of agate conducted by Masuda and Fujimura (1981), the initial fibrous texture changed completely to recrystallized quartz aggregates with Type S and Type P microstructures. Type S microstructure is characterized by flattened recrystallized grains with serrated grain boundaries, whereas Type P is defined by a mosaic texture that consists of polygonal grains with relatively straight grain boundaries. The change in grain boundary morphology from Type S to Type P was quantified by perimeter analysis (Takahashi et al., 1998).

Type S microstructure occurs at relatively low-T/high-$\dot{\varepsilon}$ conditions, whereas Type P appears at high-T/low-$\dot{\varepsilon}$ conditions (Fig. 4b). The ranges of $T-\dot{\varepsilon}$ conditions reported by Masuda and Fujimura

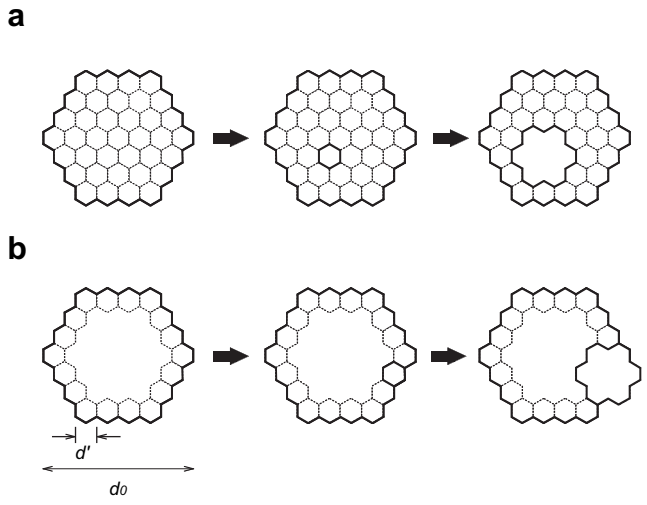

Fig. 3. Processes of continuous DRX. Solid lines represent grain boundaries and dotted lines represent subgrain boundaries. (a) Intracrystalline nucleation by SGR followed by grain growth. (b) Marginal nucleation by SGR followed by grain growth.

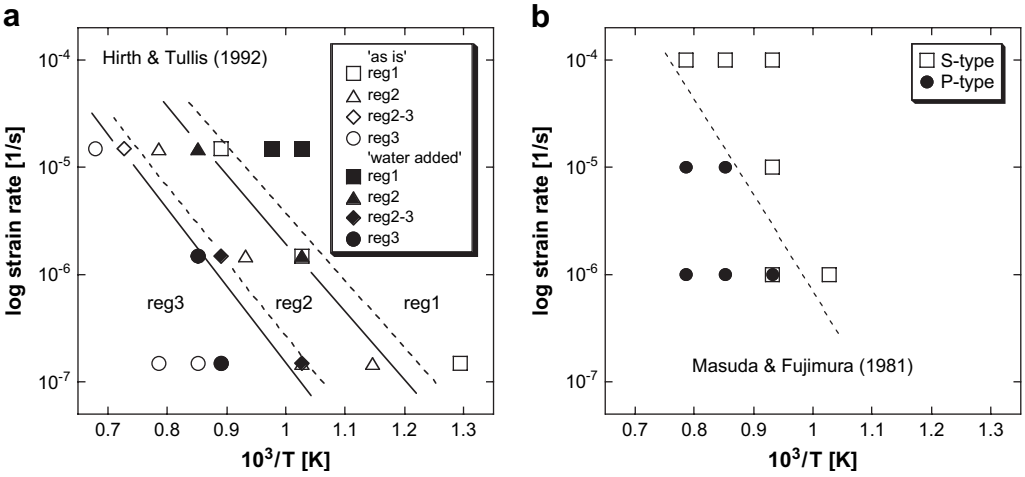

Fig. 4. Deformation and recrystallization microstructures of quartz in constant-strain-rate tests at high-*PT* conditions. (a) Regimes 1–3 after Hirth and Tullis (1992) at $P_c = 1.5$ GPa. Solid and dotted lines represent the regime boundaries for 'as is' and 'water added' quartzite samples, respectively. (b) Types S and P microstructures observed in deformation experiments of agates after Masuda and Fujimura (1981) at $P_c = 0.4$ GPa under 'wet' conditions.

(1981) largely overlap with those of Hirth and Tullis (1992), although these two sets of experiments are not strictly comparable because of differences in confining pressure P_c, sample assembly, and the water content of the samples; nevertheless, Fig. 4a and b suggests that the S–P transition occurs at conditions that correspond to Regime 2. The mechanism of the S–P transition described in these previous studies is poorly understood; however, from the viewpoint of recrystallization mechanisms, the occurrence of serrated grain boundaries in Type S samples might be related to BLG and/or marginal SGR, although internal subgrains are also visible in some previously published microphotographs.

Type S and Type P are regarded as steady-state microstructures, dependent only on the state variables of $\dot{\varepsilon}$ and T; hence, quartzite samples assigned to Regimes 1–3 would approach either Type S or Type P with increasing strain. Indeed, completely recrystallized samples in Regime 3 (e.g., Fig. 6(d) in Hirth and Tullis, 1992) are indistinguishable from the microphotographs of Type P samples presented by Masuda and Fujimura (1981). Combining these experimental results, a conceptual model of the evolution of quartz microstructures is presented for the case of $d_i < d$ (Fig. 5). For the extrapolation of the experimental conditions to natural $T-\dot{\varepsilon}$ conditions, the possible effects of d_i and ε must be taken into account, along with variations in P_c.

Quartz microstructures similar to those in Regimes 1–3, or Types S and P, are commonly observed in metamorphic belts and fault zones (e.g., Masuda, 1982; Hirth et al., 2001; Stipp et al., 2002a,b). Stipp et al. (2002a,b) divided a mylonitic fault zone into three zones based on the dominant recrystallization microstructures in quartz veins: 'bulging recrystallization (BLG)', 'subgrain rotation recrystallization (SGR)', and 'grain boundary migration recrystallization (GBM)' zones in ascending order of metamorphic grade. 'BLG' was defined in a broad sense as recrystallization at serrated grain boundaries, including the combined process of subgrain rotation and bulging at grain margins. Accordingly, the 'BLG' zone was correlated with experimental Regime 1 and the low-*T* part of Regime 2. The 'SGR' zone was correlated with the high-*T* part of Regime 2, and Regime 3 with the 'SGR'–'GBM' transition zone.

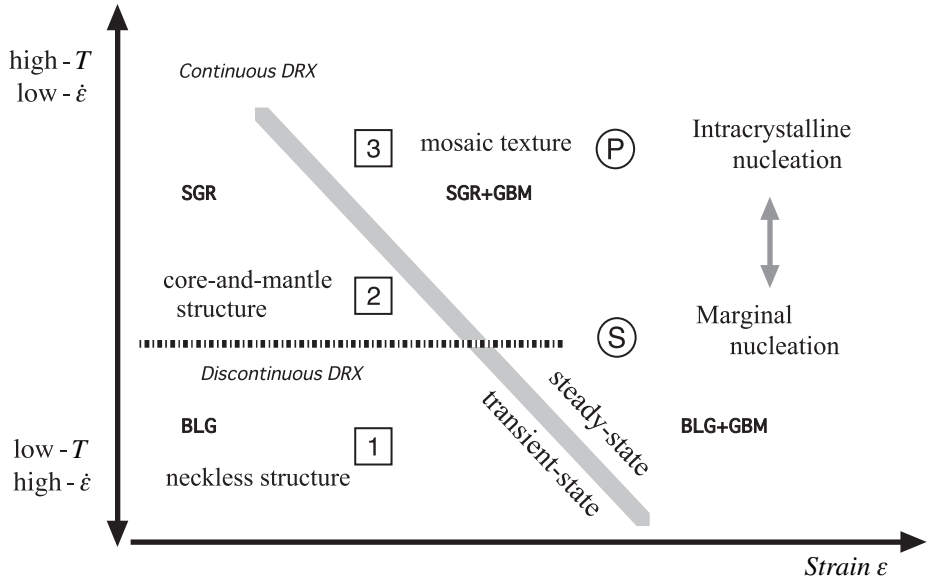

Fig. 5. Microstructural evolution of quartz in DRX. In this case, the initial grain size is assumed to be larger than that in a steady state. The numbers 1–3 represent the deformation regimes defined by Hirth and Tullis (1992), and S and P represent the microstructural types defined by Masuda and Fujimura (1981).

The 'GBM' zone is characterized by recrystallized grains with lobate and interfingering grain boundaries, and a reduced number of subgrains. Pinning and dragged microstructures are common in the low-*T* sub-zone of the 'GBM' zone, whereas large recrystallized grains with irregular amoeboid shapes and 'left-over grains' (Urai et al., 1986) characterize the high-*T* sub-zone. Although this type of recrystallization has not been reported in deformation experiments of quartz, similar microstructural features are found in a Mg-alloy deformed at high homologous temperatures (Drury et al., 1985; De Bresser et al., 1998). In the present scheme, 'GBM' of Stipp et al. (2002a,b) is classified into CDRX (SGR + GBM).

4. Theoretical basis of grain size piezometers

4.1. Static energy-balance model

The universal relations among recrystallized grain size d, subgrain size d', and flow stress σ were first treated theoretically by Twiss (1977, 1980). To derive Eq. (2) of subgrain size, Twiss assumed the following:

(i) the total length L_d of free dislocations before the formation of subgrains is the same as the length L_s of dislocations that are re-arranged in sub-boundaries;
(ii) the energy E_{sub} of a sub-boundary at the initial stage of subgrain formation is the same as the energy E_{disl} of free dislocations that were contained in the same volume; and
(iii) once subgrains are formed, their size does not change during subsequent misorientation.

Assumption (iii), of constant subgrain size, may be an over-simplification, as subgrain growth is sometimes observed in deformed minerals (Drury et al., 1985). The formulation of subgrain size proposed by Twiss (1980) is given in Appendix B. Assumptions (i), (ii), and (iii) yield Eqs. (B.1), (B.3), and (B.11) in Appendix B, respectively. The exponent $p' = 1$ of subgrain size is then derived from general dislocation theory.

Considering that new grains are formed by progressive misorientation of subgrains, Eq. (1) of recrystallized grain size was derived via a similar stability analysis; however, to allow a p value other than 1, Twiss (1977, 1980) introduced an additional parameter ϕ, defined as

$$\phi \equiv \frac{L_s}{L_d}, \tag{10}$$

which is directly related to p as

$$\frac{1}{p} = \frac{\phi}{2\phi - 1}. \tag{11}$$

While the conservation of dislocation length ($\phi = 1$) was assumed for climb-controlled subgrain formation, $\phi > 1$ was postulated for recrystallized grains. To explain the latter case, Twiss (1980) considered that dislocation-free new grains are formed by the outward expansion of dislocation loops that sweep out internal dislocations; the total length of dislocations increases during expansion of the loops. However, this process differs from the nucleation mechanisms observed in actual materials described in Section 3.2. The expansion of dislocation loops is generally considered as a mechanism of dislocation multiplication, and is understood as a mechanism of strain hardening rather than recovery. Even if this loop expansion model is accepted, it is difficult to constrain the value of ϕ, which requires knowledge of the average increase in dislocation length during the formation of a recrystallized grain. A value of 1.4–2 was tentatively chosen "as a first-order approximation" (Twiss, 1980), but there appears to be no reason to limit ϕ within this range. Twiss (1980) himself stated that "given the complexity of dislocation structures, there seems no hope of actually calculating such a value".

In the Twiss model, the only distinction between subgrains and new grains is the value of ϕ; however, the loop expansion model is unrealistic and ϕ is poorly constrained, as discussed above. Another drawback of the Twiss model is the assumption of constant grain size: the criterion of the minimum strain energy gives only the initial size of recrystallized grains, corresponding to the smallest size of 'stable' grains. This limitation has been repeatedly criticized in later works (Poirier, 1985; Derby, 1990; Shimizu, 1998b; De Bresser et al., 2001). Because nucleation-and-growth events continue to occur in DRX even after the attainment of a steady state, energetically 'stable' grains are unlikely to maintain their size over time.

In conclusion, the Twiss theory cannot be accepted as a predictive model for recrystallized grain size, while the Twiss model of subgrain size seems to be meaningful. Although Eq. (1) with $p = 1.47$ is still quoted as a "theoretical" relation of Twiss (1977), the scaling parameters p and K were in fact determined by the least-squares fitting of empirical data, most of which were obtained in metals (Cu and Cu-alloys, Ni and Ni-alloys, and α-Fe). Data for olivine and quartz (Post, 1973; Mercier et al., 1977) were also included; however, the accuracy of stress measurements in these early works was unsatisfactory. Revised d–σ relations for minerals are discussed in a later section.

4.2. Nucleation-and-growth models

In contrast to the Twiss model, in which recrystallized grains are assumed to be stable in steady-state creep, Derby and Ashby (1987) and Shimizu (1998b) considered that the sizes of individual grains vary with time and space during DRX. In their models, the average grain size was derived from a dynamic balance between nucleation-and-grain growth. Assuming that one nucleation event occurs at a grain boundary while one grain is swept out by GBM at a steady state, Derby and Ashby (1987) and Derby (1990, 1991) obtained the following scaling relation (e.g., Eq. (13.4) of Derby (1990)):

$$d = a_{gb}\left(\frac{\dot{R}}{I_{gb}}\right)^{\frac{1}{3}}, \tag{12}$$

where I_{gb} is the nucleation rate per unit area of the boundary and $a_{gb} = (2/\pi)^{1/3}$. The above scaling analysis is, however, too simple to deal with polycrystalline materials that show a wide range in grain size distribution (GSD). Shimizu (1998a, 1999) modeled the steady-state GSD that results from cyclic events of nucleation-and-growth, and derived the following scaling relation:

$$\widehat{d} = a\left(\frac{\dot{R}}{I}\right)^{\frac{1}{4}}, \tag{13}$$

where $\widehat{d}$ is the grain size that corresponds to the mode of logarithmic grain size, I is the nucleation rate per unit volume, and a is a scaling factor. From Fig. 4(a) and Fig. 5 of Shimizu (1999), $a = 1.14$ for a true 3D distribution and $a = 1.12$ for a distribution measured on a 2D section. The above equation was used by Shimizu (1998b) to formulate piezometric relations. Although Eq. (13) was derived for intracrystalline nucleation, the same scaling law holds for grain boundary nucleation provided that microstructures have reached steady states (see Appendix B of Shimizu, 1999). Indeed, substitution of $I = 3I_{gb}/d$ into Eq. (12) yields Eq. (13) with $a = 1.18$. Hence the basic scaling relation of the Derby–Ashby model is almost equivalent to that of the Shimizu model.

The scaling laws of the forms of Eqs. (12) and (13) represent the competing effects of nucleation-and-growth. The stress dependence of grain size can be evaluated if the governing equations for $\dot{R}$ and I_{gb} or I are given. For the growth rate $\dot{R}$, Derby and Ashby (1987) and Shimizu (1998b) assumed recovered microstructures and applied $j=1$ for Eq. (3). For the nucleation rate I_{gb}, Derby and Ashby (1987) considered BLG nucleation at grain boundary sites pinned by sub-boundaries (Fig. 2a); hence, their model describes the microstructures of DDRX. The grain size was finally formulated as follows (cf. Eq. (19) of Derby (1991)):

$$\frac{d}{b} = B\left(\frac{\sigma}{\mu}\right)^{-p} \exp\left(-\frac{\Delta Q}{mRT}\right), \tag{14}$$

where B is a non-dimensional constant, and

$$\Delta Q = Q_{gb} - Q_c, \quad p = \frac{n}{2}, \quad m = 2. \tag{15}$$

For typical values of stress exponents, $n=3$–5, the exponent varies as $p=1.5$–2.5. Eq. (14) predicts that the recrystallized grain size has a weak temperature dependence.

In contrast to the Derby–Ashby model, Shimizu (1998b) assumed SGR nucleation in CDRX. Using the intracrystalline or marginal SGR nucleation rate given in Appendix C, the steady-state grain size was obtained as

$$\frac{d}{b} = \tilde{B}\left(\frac{\sigma}{\mu}\right)^{-p}\left(\frac{wD_{gb}}{bD_v}\right)^{\frac{1}{m}}, \tag{16}$$

where $\tilde{B}$ is a non-dimensional constant, D_v is the volume diffusion coefficient,

$$p = \frac{5}{4} = 1.25, \quad m = 4 \tag{17}$$

for intracrystalline nucleation, and

$$p = \frac{4}{3} = 1.33, \quad m = 3 \tag{18}$$

for marginal nucleation. The full expression of $\tilde{B}$ is given in Appendix D. The temperature dependence of D_v is expressed as

$$D_v = D_v^0 \exp\left(-\frac{Q_v}{RT}\right), \tag{19}$$

where D_v^0 is a constant and Q_v is the activation energy of volume diffusion. Using Eqs. (6) and (19), Eq. (16) is re-arranged in the form of Eq. (14), with

$$B = \tilde{B}\left(\frac{wD_{gb}^0}{bD_v^0}\right)^{1/m} \tag{20}$$

and

$$\Delta Q = Q_{gb} - Q_v. \tag{21}$$

It is noted that both the theories of Derby and Ashby (1987) and Shimizu (1998b) use Eq. (2) with the exponent $p'=1$, which is consistent with Twiss's (1977, 1980) model of subgrain size (Appendix B). Edward et al. (1982) considered that subgrain size is determined by a dynamic balance between glide and climb-controlled annihilation of dislocations, thereby deriving a different scaling relation of subgrain size with $p'=n/4$. For ordinary values of $n=3$–5 in recovery-controlled creep, p' varies over the range 0.75–1.25. The use of $p'=n/4$ in place of $p'=1$ in the Derby–Ashby and Shimizu models yields p and m values slightly different from those in Eqs. (15), (17), and (18).

4.3. Simultaneous operation of dislocation and diffusion creeps

In the nucleation-and-growth models of Derby and Ashby (1987) and Shimizu (1998b), surface energy is neglected as a driving force of GBM; however, surface energy may become important if considerable grain size reduction occurs via DRX. If new grains are sufficiently small, the creep mechanism operating within these grains may switch from dislocation creep to diffusion creep. This would result in the cessation of dislocation multiplication, sub-boundary formation, and recrystallization processes other than surface-energy-driven grain growth; as a consequence, recrystallized grains would again begin to coarsen. Grain growth would continue until the grain size became large enough to switch on dislocation creep again. Following this reasoning, De Bresser et al. (1998) considered that the recrystallized grain size tends to stabilize within this boundary zone between the fields of dislocation creep and diffusion creep. The grain size at the creep mechanism boundary is calculated as follows.

Because dislocation creep and diffusion creep are parallel and concurrent processes, the strain rate is generally written as

$$\dot{\varepsilon} = \dot{\varepsilon}_{disl} + \dot{\varepsilon}_{diff}, \tag{22}$$

where $\dot{\varepsilon}_{disl}$ and $\dot{\varepsilon}_{diff}$ are the strain rates of dislocation creep and diffusion creep, respectively. The relative importance of dislocation creep with respect to diffusion creep is represented by the parameter c:

$$c \equiv \frac{\dot{\varepsilon}_{disl}}{\dot{\varepsilon}_{diff}}. \tag{23}$$

We applied Eq. (8) to $\dot{\varepsilon}_{disl}$, although some minerals such as calcite deform by mechanisms other than recovery-controlled dislocation creep and thereby do not obey the power law (De Bresser, 2002; Renner and Evans, 2002; Renner et al., 2002). The strain rate of diffusion creep is given by

$$\dot{\varepsilon} = \frac{42VD}{RTd^2}\sigma, \tag{24}$$

where V is the molar volume, $D=D_v$ for Nabarro–Herring creep, and $D=(\pi/d)wD_{gb}$ for Coble creep (Frost and Ashby, 1982). The grain size at the creep mechanism boundary ($c=1$) is then written in the same form as Eq. (14), with

$$\Delta Q = Q_v - Q_c, \quad m = 2, \quad p = \frac{n-1}{2} \tag{25}$$

for the boundary between dislocation creep and Nabarro–Herring creep, and

$$\Delta Q = Q_{gb} - Q_c, \quad m = 3, \quad p = \frac{n-1}{3} \tag{26}$$

for the boundary between dislocation creep and Coble creep.

When polycrystalline aggregates are saturated with fluids and pressure solution is active, the flow law of pressure solution creep (or solution-precipitation creep) is used for $\dot{\varepsilon}_{diff}$ (Ter Heege et al., 2005a). Because the flow law of diffusion-controlled pressure solution creep is written in a similar form to that of Coble creep (e.g., Eq. (43) of Shimizu, 1995), the scaling parameters are also given by Eq. (26) with the activation energy Q_{gb} for wet grain boundaries, whereas in the case of pressure solution controlled by the rate of dissolution or precipitation at the solid–fluid interface the scaling parameters are given by $\Delta Q = Q_r - Q_c$, $m=1$, and $p=n-1$, where Q_r is the activation energy for dissolution or precipitation of the solid. The latter case is easily derived by applying the flow law of the form of Eq. (44) of Shimizu (1995) to $\dot{\varepsilon}_{diff}$.

The basic assumption of the field boundary model of De Bresser et al. (1998) is that the average grain size is always reduced by DRX in the dislocation creep field, whereas grain growth occurs in the diffusion creep field; however, DRX involves not only the processes of grain size reduction but also grain growth driven by strain energy and surface energy. If grain size is stabilized within the dislocation creep field by these competitive processes, as modeled by Derby and Ashby (1987) and Shimizu (1998b), it never reaches the diffusion creep field; therefore, the boundary between the fields of dislocation and diffusion creep is regarded as the lower bound of steady-state grain size.

Austin and Evans (2007) formulated steady-state grain size from a dynamic balance between grain boundary formation and grain growth, and demonstrated scaling parameters slightly different from those in Eq. (26). Their approach is similar to the nucleation-and-growth models of Derby and Ashby (1987) and Shimizu (1998b); however, they ignored strain energy as a driving force of grain growth and used the kinetic law of normal grain growth driven by surface energy. Hence, the model itself is somewhat similar to the field boundary model of De Bresser et al. (1998), although in the Austin–Evans model the grain size is not constrained to lie at the creep mechanism boundary. It is questionable as to whether the growth law under static conditions can be applied to DRX in the dislocation creep field, where strain energy is generally larger than surface energy (see Section 3.1). For the process of grain size reduction, the authors simply assumed that the area of new grain boundaries produced by deformation is proportional to the work done by external forces in steady-state dislocation creep. Because of an unknown parameter introduced in this hypothesis, their scaling relations cannot be used for paleostress analysis (see Appendix E).

While the hypothesis of De Bresser et al. (1998) and the scaling assumption of Austin and Evans (2007) lack a grounding in physical modeling of recrystallization processes and an explanation of log-normal GSDs, possible surface energy effects are neglected in the Derby–Ashby and Shimizu models. The development of an integrated model, including both the effects of deformation and surface energy, is therefore required in future studies.

5. Comparison of theories and experimental data

5.1. Stress exponents in scaling relations

As summarized in the previous section, the predictive models of recrystallized grain size proposed to date include the Derby–Ashby model (Derby and Ashby, 1987; Derby, 1990, 1991) of BLG nucleation and strain-induced GBM, corresponding to DDRX, the Shimizu model (Shimizu, 1998b, 1999) of SGR nucleation and strain-induced GBM, corresponding to CDRX, and the field boundary model of De Bresser et al. (1998, 2001). The d–σ relations derived from these theories are represented by Eq. (14), although with slightly different stress exponents and degrees of temperature dependence for each. The similar nature of the different forms of the d–σ relations arises from the fact that all of these theories model the competing processes of deformation-induced grain size reduction and grain growth driven by strain energy or surface energy. Because Q_c and Q_v are larger than Q_{gb} for most materials, ΔQ in Eqs. (15), (21), and (26) is generally negative; hence, a weak negative temperature dependence of grain size is predicted from the Derby–Ashby model, the Shimizu model, and the field boundary model for the case of the boundary between the fields of dislocation creep and Coble creep.

The classification of DRX mechanisms and corresponding theories are summarized in Table 1. Some authors (De Bresser et al., 2001; Stipp et al., 2006) have argued that the Derby–Ashby model corresponds to 'migration' recrystallization, whereas the Shimizu model was labeled 'rotation' recrystallization; however, this is not the case. The former models BLG + GBM (i.e., steady states of DDRX), whereas the latter models SGR + GBM (i.e., steady states of CDRX); thus, both can be assigned to 'migration' in the sense of Poirier (1985). The grain size after 'rotation' recrystallization (i.e., transient state of CDRX) would be approximated by a subgrain size d', for which theoretical models have been provided by Twiss (1977, 1980) and Edward et al. (1982).

In the Derby–Ashby model and the field boundary model, the exponent p is related to the stress exponent n of recovery creep, whereas p of the Shimizu model is not. To test the theoretical models, experimentally determined values of p are plotted against n determined in the same deformation experiment, or n in other experiments with similar conditions (Fig. 6a). The plots are basically the same as those in Fig. 5 of De Bresser et al. (2001); however, recent experimental results for quartz (Stipp and Tullis, 2003) and halite (Ter Heege et al., 2005a) have been added to the plots in the present paper, and data for which the original papers were unpublished or are currently inaccessible are omitted. The works of Friedman and Higgs (1981) on calcite and Jacka and Li (1994) on ice are also omitted because of the high degree of scatter in the original data. The data sources are listed in Table 2. Note that in all works except for De Bresser et al. (1998) and Ter Heege et al. (2005a), grain size data obtained at different temperature conditions were merged to be fitted to Eq. (1), although recent theories predict a weak temperature dependence of d.

The sizes of recrystallized grains have been measured using several different methods, including the linear intercept method (Karato et al., 1980; Drury et al., 1985; van der Wal et al., 1993; Post and Tullis, 1999) and the area counting method. In the latter case, the representative grain size is defined by the geometric mean (e.g., Stipp and Tullis, 2003; Ter Heege et al., 2005a), the median equivalent circular diameter (Ter Heege et al., 2005a), or the mean square diameter (Rutter, 1995). The linear intercept method is one of the conventional methods used to determine the mean grain size from a photomicrograph; however, the precise determination of the stereologic factor requires knowledge of GSD (log-normality is generally assumed) and grain shapes (equiaxed polygonal grains are generally assumed). To compare empirical data with the theoretical predictions of Derby and Ashby (1987) and Shimizu (1998b), it is best to use the diameter that corresponds to the mode of logarithmic grain size, denoted by $\hat{d}$ in Eq. (13). In general, steady-state GSDs in DRX are close to log-normal (Shimizu, 1998a, 1999,

Table 1
Classification of DRX mechanisms and applicability of grain size models

DRX	State	Mechanism	Grain size model	p	m	ΔQ
DDRX	Steady	BLG + GBM	Derby and Ashby (1987)	$n/2$	2	$Q_{gb} - Q_c$
CDRX	Transient	SGR	Twiss (1977)	1[a]	–	–
	Transient	SGR	Edward et al. (1982)	n/4[a]	4	$Q_v - Q_c$
	Steady	Marginal SGR + GBM	Shimizu (1998b)	1.33	3	$Q_{gb} - Q_v$
	Steady	Intracrystalline SGR + GBM	Shimizu (1998b)	1.25	4	$Q_{gb} - Q_v$
Any	Steady	DRX + Nabarro–Herring creep	De Bresser et al. (1998)	$(n-1)/2$	2	$Q_v - Q_c$
	Steady	DRX + Coble creep	De Bresser et al. (1998)	$(n-1)/3$	3	$Q_{gb} - Q_c$

[a] Values for subgrain size.

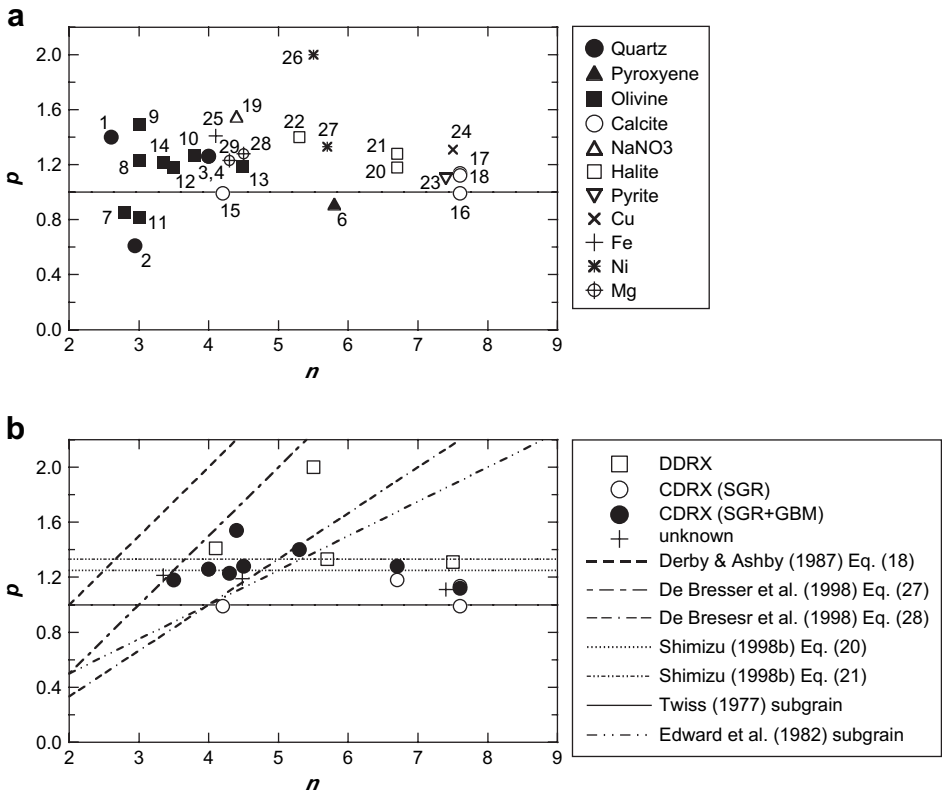

Fig. 6. (a) Stress exponent p of recrystallized grain size plotted against the power law exponent n of dislocation creep for a wide range of materials, after Table 2. Numbers correspond to the data sources listed in Table 2. (b) Comparison of scaling parameters p and n calibrated in laboratory studies and those predicted theoretically. The data obtained from solid-medium apparatus are omitted. DRX mechanisms are classified according to Fig. 1.

2003) and the median grain size is close to $\hat{d}$, whereas the mean diameter deviates to larger values (Ter Heege et al., 2002, 2005a,b). Differences in the methods of grain size analysis might have caused some bias in calibration of the experimental relations; nevertheless, to make use of data from various materials, the details of the measurement and averaging methods are neglected in Fig. 6.

The empirical data compiled in Fig. 6a show a large degree of scatter overall. The data that plot in the range of $p \leq 0.9$ were all obtained from Griggs-type apparatus with solid confining media (Table 2), for which accurate stress measurements are difficult and thus the reliability of p and n is uncertain. Ignoring these data, there appears to be no correlation between p and n. In Fig. 6b, the data from solid-medium apparatus are omitted and the remaining data are compared with theoretical predictions. The data with large n, such as those for calcite (Schmid et al., 1980; Rutter, 1995), deviate significantly from the ranges predicted according to the Derby–Ashby model and the field boundary model of De Bresser et al. (1998). The most reliable data of olivine (Karato et al., 1980; van der Wal et al., 1993), calcite (Rutter, 1995), halite (Ter Heege et al., 2005a), and quartz (Stipp and Tullis, 2003) plot within a narrow band at around $p = 1.25$ (± 0.15), consistent with the theoretical prediction of the Shimizu model.

In Fig. 6b, DRX mechanisms are classified as either DDRX or CDRX based on the relative importance of BLG and SGR nucleation, and the latter is further divided into SGR and SGR + GBM based on the activity of GBM (Fig. 1). As illustrated in Fig. 5, Regimes 1, 2, and 3 of quartz (Stipp and Tullis, 2003) and feldspar (Post and Tullis, 1999) are referred to as DDRX, CDRX (SGR), and CDRX (SGR + GBM), respectively. The DRX mechanisms for other minerals are identified based on descriptions such as 'rotation' or 'migration', and photomicrographs presented in the original papers. The data described originally as 'rotation' are here classified as CDRX (SGR), and the 'migration' recrystallization that occurred on the high-T side of 'rotation' recrystallization (e.g., Guillopé and Poirier, 1979; Tungatt and Humphreys, 1984) or that occurred subsequent to 'rotation' recrystallization (Rutter, 1995) is inferred to be CDRX (SGR + GBM). Schmid et al. (1980) observed both subgrain formation and extensive grain growth in their deformation experiments on marble, indicating CDRX (SGR + GBM); however, because they selected equiaxed new grains for grain size analysis and ignored grains that had undergone growth following nucleation, their data are classified as CDRX (SGR). The data of Karato et al. (1980) on olivine are assigned to CDRX (SGR + GBM) because the experiments were conducted at relatively high temperatures (1500–1650 °C) and because recrystallized grains were much larger than subgrains. Cu, α-Fe, Ni, and Ni-alloys show remarkable strain weakening and oscillation in stress–strain curves (Luton and Sellars, 1969; Glover and Sellars, 1973; Sah et al., 1974; Blaz et al., 1983), which is typical of DDRX. Recrystallization of a Mg-alloy is characterized by mosaic textures resulting from subgrain formation and the migration of grain boundaries (Drury et al., 1985; De Bresser et al., 1998; Drury and Urai, 1990), thereby warranting classification as CDRX (SGR + GBM).

The exponent p of minerals identified as SGR + GBM in Fig. 6b is well explained by the Shimizu model, although the data for $NaNO_3$ (Tungatt and Humphreys, 1984) deviate from the theoretical predictions. The size of new grains formed by SGR is comparable to that predicted by the subgrain models, as stated above (Table 1). Recrystallized grains of calcite resulting from SGR (Schmid et al., 1980) exhibit $p \simeq 1$ regardless of the flow law exponent n, which is consistent with the Twiss model of subgrain size rather than the model proposed by Edward et al. (1982). The DDRX data (BLG ± GBM) do not show any trend as a whole, but data obtained from metals all plot around or above $p = 1.3$ regardless of n-values. Data with $p < 1$ are reported from Regime 1 of quartz (unpublished B. Sc. thesis of R. R. Bishop after Stipp and Tullis (2003)) and albitic

Table 2
Compilation of experimentally determined values of stress exponents p and n

	Crystal	Material	p	n	Mechanism	P_c media	Source
1	Quartz	Quartzite, wet	1.40			Solid	Mercier et al. (1977)
		Canyon Creek quartzite, wet		2.6		Solid	Parrish et al. (1976)
2	Quartz	Novaculite, as-is	0.61		DDRX	Solid	Stipp and Tullis (2003)
		Black Hills quartzite, as-is		*2.9*	DDRX	Molten salts	Gleason and Tullis (1995)
3	Quartz	Black Hills quartzite, as-is	1.26		SGR	Molten salts	Stipp and Tullis (2003)
		Black Hills quartzite, as-is		4.0	SGR	Molten salts	Gleason and Tullis (1995)
4	Quartz	Black Hills quartzite, as-is	1.26		SGR + GBM	Molten salts	Stipp and Tullis (2003)
		Black Hills quartzite, as-is		4.0	SGR + GBM	Molten salts	Gleason and Tullis (1995)
5	Albite	Hot pressed powder	0.66	*0.62*[a]	DDRX	Solid	Post and Tullis (1999)
6	Pyroxene	Websterite, dry	0.90	5.8		Solid	Avé Lallemant (1978)
7	Pyroxene	Enstatite, wet	0.85	2.8		Solid	Ross and Nielson (1978)
8	Olivine	Mt. Burnet dunite, dry, wet	1.23			Solid	Mercier et al. (1977)
		Mt. Burnet dunite, dry, wet		3.0		Solid	Post (1977)
9	Olivine	Mt. Burnet dunite, dry	1.49	3.0		Solid	Post (1977)
10	Olivine	Mt. Burnet dunite, dry	1.27	3.8		Solid	Ross et al. (1980)
11	Olivine	Mt. Burnet dunite, wet	0.82			Solid	Ross et al. (1980)
		Mt. Burnet dunite, wet		3.0		Solid	Post (1977)
12	Olivine	San Carlos olivine, dry	1.18		SGR + GBM	None	Karato et al. (1980)
		San Carlos olivine, dry		3.5		Gas	Karato et al. (1986)
13	Olivine	Åhiem dunite, wet	*1.19*			Gas	van der Wal et al. (1993)
		Åhiem dunite, wet		4.48		Gas	Chopra and Paterson (1984)
14	Olivine	Anita Bay dunite, wet	*1.21*			Gas	van der Wal et al. (1993)
		Anita Bay dunite, wet		3.35		Gas	Chopra and Paterson (1984)
15	Calcite	Carrara marble	0.99	4.2	SGR	Gas	Schmid et al. (1980)
16	Calcite	Carrara marble	0.99	7.6	SGR	Gas	Schmid et al. (1980)
17	Calcite	Carrara marble	1.14		SGR	Liquid, gas	Rutter (1995)
		Carrara marble		7.6		Gas	Schmid et al. (1980)
18	Calcite	Carrara marble	1.12		SGR + GBM	Liquid, gas	Rutter (1995)
		Carrara marble		7.6		Gas	Schmid et al. (1980)
19	$NaNO_3$	Hot pressed powder	1.54	4.4	SGR + GBM	None	Tungatt and Humphreys (1984)
20	Halite	Single crystal	1.18	6.7	SGR	None	Guillopé and Poirier (1979)
21		Single crystal	1.28	6.7	SGR + GBM	None	Guillopé and Poirier (1979)
22	Halite	Sintered aggregate, wet	1.40[b]		SGR + GBM	Liquid	Ter Heege et al. (2005a)
		Avery Island rocksalt, dry		5.3		Liquid	Carter et al. (1993)
23	Pyrite	Blow orebody	1.11	*7.4*		Gas	Cox et al. (1981)
24	Cu		*1.31*	7.5	DDRX	None	Blaz et al. (1983)
25	Fe	Ferrite (α)	1.41	4.1	DDRX	None	Glover and Sellars (1973)
26	Ni		2.0	*5.5*	DDRX	None	Sah et al. (1974)
27	Ni-Fe alloy	0–20% Fe	1.33	5.7	DDRX	None	Luton and Sellars (1969)
28	Mg-alloy	Magnox Al80	1.28	4.5	SGR + GBM	None	Drury et al. (1985)
29	Mg-alloy	Magnox Al80	1.23	4.3	SGR + GBM	None	De Bresser et al. (1998)

The italicized values represent the value not explicitly presented in the original paper, and determined by linear regression of the original data or quantified graphically by the author.
[a] Not used for Fig. 6 because of large error bars.
[b] The value determined for the median grain size.

feldspar (Post and Tullis, 1999). These data must be interpreted with caution because the problem of internal friction in the solid-medium assembly was not resolved in these experiments; in addition, only small parts of the host grains were recrystallized in Regime 1, even though existing theoretical models assume steady-state microstructures with complete recrystallization. From a theoretical viewpoint, it is possible that the piezometric relation changes for different DRX mechanisms; however, additional experimental evidence is required to demonstrate the validity of this idea.

5.2. Recrystallized grain size versus deformation mechanism maps

As demonstrated above, the exponent p of minerals is most successfully explained by the Shimizu model, although some data are also compatible with the field boundary model. De Bresser et al. (1998, 2001) and Ter Heege et al. (2005a,b) plotted the mean grain sizes of calcite, olivine, and wet halite on deformation mechanism maps (in d–σ space at fixed T) for each mineral, thereby supporting their field boundary model. In a strict sense, the mean grain size in terms of number frequency is inappropriate for the field boundary model because it does not necessarily coincide with the grain size class of the largest volume fraction, which is most dominant in the flow law of a material with a distributed grain size (Freeman and Ferguson, 1986; Ter Heege et al., 2004). Instead, the use of the grain size class with the largest intersection area would be a better approach. This size class is significantly larger than the mean or median grain size defined in terms of number frequency (Ter Heege et al., 2002, 2005a,b), when steady-state GSDs are attained in DRX. Deformation mechanism maps should also be constructed from diffusion creep flow laws calibrated for the volume-based or intersection-area-based average of grain sizes. Accurate comparisons between the recrystallized grain sizes of these minerals and deformation mechanism maps using appropriate averaging methods remain a task for future studies.

Here, the recrystallized grain size of quartz is examined, for which well-constrained data were recently obtained by Stipp and Tullis (2003) using a Griggs-type apparatus with a molten salt cell. The boundary between the dislocation and diffusion creep fields can be calculated from the flow law parameters determined by Rutter and Brodie (2004a,b), who conducted a series of deformation experiments on hot pressed quartz aggregates using a gas-medium apparatus (Table 3). The result of the calculation (Fig. 7) reveals that diffusion creep is only dominant for very fine-grained quartz (up to 3 μm in volume-based averages) under low differential stress (up to 30 MPa). However, it is questionable as to whether the rheological data of Rutter and Brodie (2004a,b) obtained at 300 MPa confining pressure

Table 3
Parameters used for calculation on quartz

Parameter	Value	Remarks	Source
α	3	Olivine, quartz	Kohlstedt and
β	3		Weathers (1980)
μ	4.2×10^4 MPa		Twiss (1977)
ν	0.15		Twiss (1977)
b	5×10^{-4} μm		Twiss (1977)
K'	7.8	Calculated by Eq. (A.23)	Pennock et al.
θ	2°	Halite	(2005)
θ_c	12°		
V	2.370×10^{-5} m^3 mol^{-1}	β-quartz	Berman (1988)
Dislocation creep of β-quartz			
A	1.1×10^{-4} MPa^{-n} s^{-1}	Black Hills quartzite,	Gleason and Tullis
n	4	without melt	(1995)
Q_c	223 kJ mol^{-1}		
Dislocation creep of β-quartz			
A	$300 \times 10^{-4.93}$ MPa^{-n} s^{-1}	Brazilian quartz	Rutter and Brodie
n	2.97	(hot-pressed aggregates)	(2004a)
Q_c	242 kJ mol^{-1}		
Diffusion creep[a] of β-quartz			
A	0.4/d(μm)^2 MPa^{-1} s^{-1}	Brazilian quartz	Rutter and Brodie
n	1	(hot-pressed aggregates)	(2004b)
Q_c	220 kJ mol^{-1}		
Oxygen diffusion in β-quartz			
D_v^0	4×10^{-11} m^{2}s^{-1}	Brazilian quartz, $\|\|$ c-axis	Giletti and Yund
Q_v	142 kJ mol^{-1}		(1984)
wD_{gb}^0	2.6×10^{-17} m^3 s^{-1}	Arkansas novaculite	Farver and Yund
Q_{gb}	113 kJ mol^{-1}		(1991b)
Oxygen diffusion in α-quartz			
D_v^0	2.9×10^{-5} m^2 s^{-1}	Brazilian quartz, $\|\|$ c-axis	Farver and Yund
Q_v	243 kJ mol^{-1}		(1991a)
wD_{gb}^0	1.7×10^{-12} m^3 s^{-1}	Calculated in this	
Q_{gb}	193.4 kJ mol^{-1}	paper (see text)	

[a] The flow law is written in the form of Eq. (8).

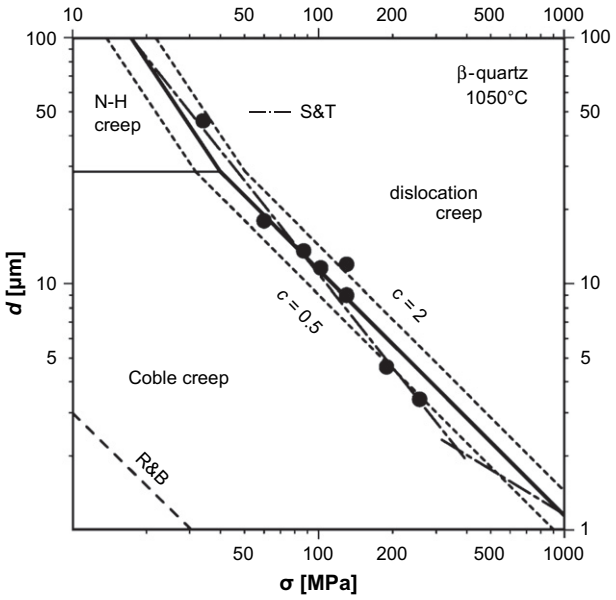

Fig. 7. Comparison of the deformation mechanism map for β-quartz at 1050 °C and the recrystallized grain size at 1000–1100 °C (solid circles) after Stipp and Tullis (2003). S&T: empirical d–σ relations within the temperature range of 700–1100 °C after Stipp and Tullis (2003). The boundaries between the deformation mechanisms of dislocation creep and diffusion creep (thick solid line) and the iso-c line (short dotted lines), and the boundary between Nabarro–Herring (N–H) creep and Coble creep (thin lines) are calculated from the dislocation creep flow law of 'as-received' quartzites after Gleason and Tullis (1995) and the oxygen diffusion coefficients in 'wet' quartz (Giletti and Yund, 1984; Farver and Yund, 1991b). R&B: boundary between the dislocation and diffusion creep fields calculated from the flow law parameters of 'dry' quartz, after Rutter and Brodie (2004a,b). The parameters used in the calculation are listed in Table 3.

can be compared with the grain size data of Stipp and Tullis (2003) obtained at 1.5 GPa. The water fugacity f_{H_2O} in the experiments of Rutter and Brodie (2004a,b) would have been very low because of small P_c and the occurrence of a redox reaction between water and iron jackets; this reaction consumes H_2O and produces H_2-rich vapors in pore spaces. In addition, the water contents of the two sets of starting materials differed by two orders of magnitudes: 10–20 H/10^6Si in the Brazilian quartz used by Rutter and Brodie (2004a,b) and several thousand H/10^6Si in the Black Hills quartzite (Gleason and Tullis, 1995) used by Stipp and Tullis (2003). In sample preparation, water adsorbed on the powdered Brazilian quartz was incorporated into the grains that displayed rapid coarsening during hot pressing; however, the total water contents after deformation remained in the range of 100–200 H/10^6Si (Rutter and Brodie, 2004a). Therefore, the water-weakening effects would have been minor in the experiments conducted by Rutter and Brodie (2004a,b). In fact, the diffusion creep flow law calibrated in their experiments is consistent with a theoretical diffusion creep flow law with the D_v value of 'dry' oxygen diffusion in quartz (Fig. 10 of Rutter and Brodie, 2004b).

A deformation mechanism map is now considered under H_2O-rich conditions. For dislocation creep of β-quartz, the flow law parameters of Gleason and Tullis (1995) are employed, whose sample assembly and experimental conditions were similar to those of Stipp and Tullis (2003). Gleason and Tullis (1995) presented flow laws for samples 'with melt' and 'without melt'. Although the activation energy determined for the former ($Q_c = 137 \pm 34$ kJ/mol) is much smaller than that for the latter ($Q_c = 223 \pm 56$ kJ/mol), the difference in strain rate is not large at high temperatures above 1000 °C. In the present analysis, the flow law for the melt-free samples is employed.

For diffusion creep, the self-diffusion coefficient D_v of oxygen in β-quartz (Giletti and Yund, 1984) and the effective grain boundary coefficient wD_{gb} in fine-grained quartz aggregates measured under 'wet' conditions (Farver and Yund, 1991b) are employed. Because oxygen diffusion in quartz is faster than silicon diffusion by a factor of 2 or 3 (Farver and Yund, 2000), the strain rate of diffusion creep estimated here is considered to represent an upper limit. Oxygen diffusion and recovery-controlled creep of quartz are both dependent on f_{H_2O} (Farver and Yund, 1991a; Paterson, 1989). Hence, it is desirable to use diffusion coefficients and a dislocation creep law obtained in similar chemical environments. The diffusion data were obtained under hydrothermal conditions with a water pressure of 100 MPa, whereas the deformation experiments of Gleason and Tullis (1995) were conducted at much higher confining pressures (about 1.5 GPa). In the latter case, water fugacity was poorly controlled, and their 'as-received' quartzite samples were not saturated with water (Hirth et al., 2001). Although water pressure and the chemical environments in the oxygen diffusion experiments (Giletti and Yund, 1984; Farver and Yund, 1991b) were not the same as those in the deformation experiments (Gleason and Tullis, 1995), the present study does not make any correction for f_{H_2O}.

The deformation mechanism map of β-quartz at 1050 °C in Fig. 7 was constructed based on the flow law parameters and diffusion data listed in Table 3. The grain size data of Stipp and Tullis (2003) appear to be concordant with the field boundary between dislocation creep and diffusion creep; however, if silicon diffusion in quartzite is slower than oxygen diffusion, the dislocation creep field would extend further downward. For example, if D_v and D_{gb} of silicon were less than the oxygen diffusion coefficients by a factor of 2, the field boundary would shift to the position of the $c = 0.5$ line in Fig. 7. It should be noted that each data point in Fig. 7 represents the geometric mean of the diameters of recrystallized grains; accordingly, the average grain size in terms of volume fraction would be shifted toward the dislocation creep field. Moreover, most of the run products described by Stipp and Tullis (2003) contained

porphyroclasts of quartz grains (with an original grain size of about 100 μm) that were excluded from their grain size analysis. Therefore, the volume-based average of whole grains would have been much larger than the reported value. In particular, in samples deformed at high stress, only the margins of original grains were replaced by recrystallized grains (Stipp and Tullis, 2003; Fig. 3a). The question of whether the field boundary model can be applied to each of the recrystallized grains in these porphyroclastic rocks remains unclear. It seems that dislocation creep was dominant in these samples and that the grain size was not effectively constrained by the rheological boundary.

6. Grain size piezometer for quartz

This section investigates how recrystallized grain size can be constrained from the nucleation-and-growth model of Shimizu (1998b, 1999). While the Shimizu model does not explicitly include flow law parameters of dislocation creep such as n, diffusion-controlled dislocation climb is assumed as an elementary process of nucleation. In this sense, recrystallized grain size in the high-temperature creep of quartz is suitable as a test case of the Shimizu model because a stress exponent of $n = 4$ (Luan and Paterson, 1992; Gleason and Tullis, 1995) is compatible with $n = 3$–5 of climb-controlled recovery creep (Poirier, 1985) and because $Q_c \simeq 150$ kJ/mol of wet quartz (Luan and Paterson, 1992) is comparable with $Q_v = 142$ kJ/mol of oxygen diffusion (Giletti and Yund, 1984).

For the parameters of diffusion in Eqs. (20) and (21), D_v and D_{gb} of oxygen in β-quartz are employed, as listed in Table 2. (D_{gb} of the fine-grained quartz aggregate corresponds to diffusion *parallel* to grain boundaries. In a strict sense, D_{gb} *across* the boundary is required, because the grain boundary diffusion coefficient in the Shimizu model is related to GBM). Because D_{gb} of silicon in quartz is slower than that for oxygen by a factor of 2 or 3 (Farver and Yund, 2000), silicon diffusion is generally assumed to be the rate-controlling process of recrystallization in quartz. D_v of silicon in 'wet' quartz would also be less than that for oxygen by a small factor, although no data are currently available for silicon diffusion in 'wet' quartz. Because diffusion data are incorporated in Eq. (16) as D_{gb}/D_v, the results of the present calculation based on oxygen diffusion would not differ significantly from those calculated based on the diffusion coefficients of silicon.

As stated in the previous section, the diffusivity of oxygen in quartz is dependent on water fugacity; however, because water promotes both D_v and D_{gb} in Eq. (16), the effects of water on recrystallized grain size are largely cancelled out. Stipp et al. (2006) recently performed experiments on 'dry' and 'water added' quartzite, but found no appreciable difference between the results of these experiments and those of previous runs using 'as-received' quartzite. It is therefore considered that the effects of f_{H_2O} on recrystallized grain size can be neglected for quartz as a first-order approximation, although for experimental studies on olivine, the effects of water on recrystallized grain size remain a topic of debate (van der Wal et al., 1993; Jung and Karato, 2001).

The present theory describes the processes of SGR + GBM that correspond to Regime 3 of quartz (Table 1; Fig. 5). Because SGR occurs within quartz grains in Regime 3, the intracrystalline nucleation model is applied. The scaling factor $\tilde{B}$ in Eq. (16) is evaluated in Appendix D using the material constants listed in Table 3. The apparent activation energy $\Delta Q/m$ is estimated to be −7.25 kJ/mol, and the steady-state grain size d [μm] is written as a function of σ [MPa] and T [K]:

$$d = 1.52 \times 10^3 \times \sigma^{-1.25} \exp\left(\frac{8.72 \times 10^2}{T}\right). \quad (27)$$

For piezometric applications, the following form would be useful:

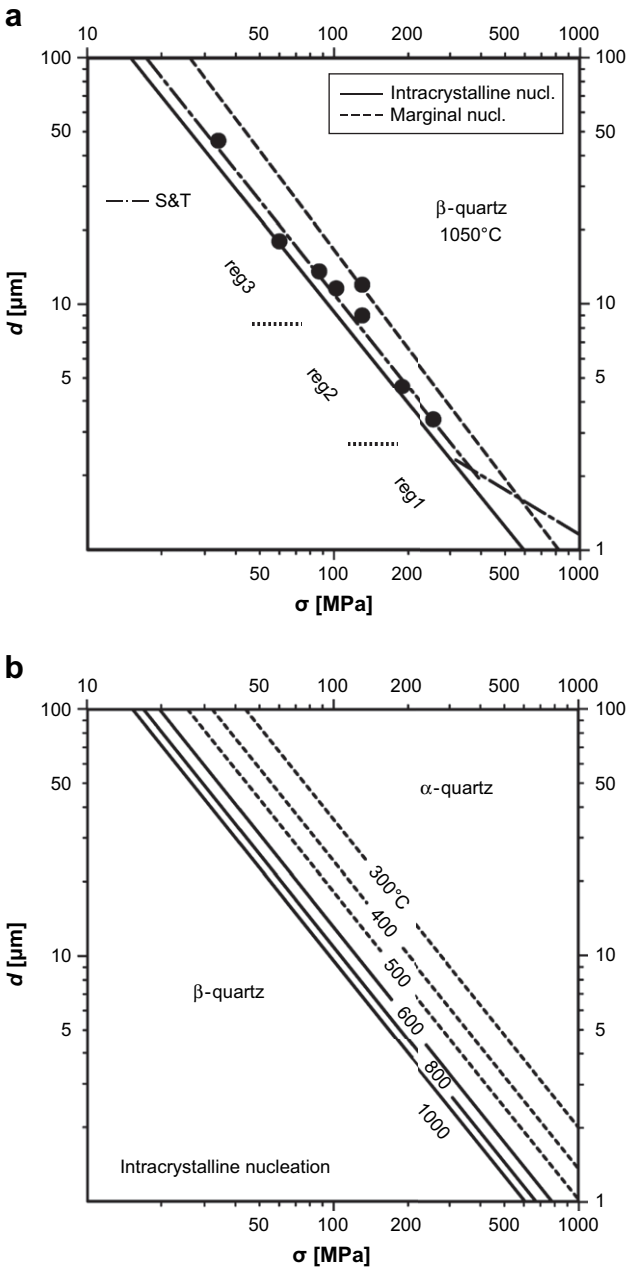

Fig. 8. Recrystallized grain size of quartz predicted by the nucleation-and-growth model of Shimizu (1998b). (a) Comparison between the theoretical prediction for β-quartz at 1050 °C and the experimental results of Stipp and Tullis (2003). Solid line: intracrystalline SGR + GBM model. Dotted line: marginal SGR + GBM model. Solid circles: recrystallized grain size at 1000–1100 °C after Stipp and Tullis (2003). S&T: empirical d–σ relations across the temperature range of 700–1100 °C, after Stipp and Tullis (2003). (b) Theoretically predicted d–σ relations for β-quartz (solid lines, 1000–600 °C) and α-quartz (dotted lines, 500–300 °C) using the intracrystalline SGR + GBM model. The transition temperature of quartz under $P_c = 100$ MPa for this calculation is 599 °C.

$$\sigma = 3.52 \times 10^2 \times d^{-0.8} \exp\left(\frac{6.98 \times 10^2}{T}\right). \quad (28)$$

The d–σ relations calculated at 1050 °C are presented in Fig. 8a. The results of the marginal nucleation model are also shown. Despite the uncertainty involved in scaling factors such as K', the grain size predicted by the intracrystalline nucleation model is in reasonable agreement with the laboratory data of Stipp and Tullis (2003) in Regime 3, whereas the results derived from the marginal nucleation model deviate on the side of higher stress.

It is noteworthy that the steady-state grain size predicted in Fig. 8a lies close to the boundary between the fields of dislocation and diffusion creep calculated from the same diffusion data (Fig. 7). At relatively low stress, corresponding to Regime 3, the steady-state grain size almost coincides with this boundary. If quartzite is deformed by dislocation creep at the conditions of Regime 3 and recrystallized via the nucleation-and-growth mechanism described by the Shimizu model, the average grain size $\hat{d}$ would approach the solid line in Fig. 8a, and the GSD would become approximately log-normal (Shimizu, 1999). Accordingly, about half of the grains fall into the diffusion creep field, and the other half remain in the dislocation creep field. This result suggests a non-trivial contribution of diffusion creep components in the composite flow law (Ter Heege et al., 2004); nevertheless, because the volume-based average size is larger than $\hat{d}$ in log-normal GSDs, dislocation creep will still be dominant at steady states. At higher stresses, corresponding to Regimes 1–2, the boundary between dislocation and diffusion creeps is located above the d–σ relation of the intracrystalline nucleation model. It is possible that diffusion creep becomes active before recrystallized grains attain the steady-state grain size of the Shimizu model. If deformation is largely accommodated by diffusion creep, surface-energy-driven grain growth may be activated and recrystallized grains may be stabilized in the area around the field boundary (De Bresser et al., 1998). The inclusion of surface energy effects is essential for further development of the theory of recrystallized grain size at high stress.

Eqs. (27) and (28) are not applicable to quartz rocks deformed in the α-quartz stability field, as Q_v of oxygen diffusion changes at the α–β transition (Giletti and Yund, 1984; Farver and Yund, 1991a). Here, the piezometric relation of α-quartz is calibrated. It is possible that Q_{gb} as well as Q_v of oxygen change at the α–β transition, although this was not verified in the diffusion experiments of Farver and Yund (1991b) over the temperature range of 450–800 °C. Here, Q_{gb} of α-quartz is calculated by assuming that the ratio of activation energy Q_v/Q_{gb} in α-quartz is the same as that in β-quartz and that D_{gb} is continuous at the transition temperature (599 °C at 100 MPa). The parameters used for α-quartz are also listed in Table 3. If no correction is made for Q_{gb} and the values of Farver and Yund (1991b) are used directly, the calculated grain size increases; hence, the present estimate is considered to be conservative.

Using the intracrystalline nucleation model, the apparent activation energy is calculated to be $\Delta Q/m = -12.4$ kJ/mol, and the recrystallized grain size of α-quartz is expressed as

$$d = 8.31 \times 10^2 \times \sigma^{-1.25} \exp\left(\frac{1.49 \times 10^3}{T}\right). \quad (29)$$

The piezometric relation for α-quartz is obtained as

$$\sigma = 2.17 \times 10^2 \times d^{-0.8} \exp\left(\frac{1.19 \times 10^3}{T}\right). \quad (30)$$

The d–σ relations calculated for α- and β-quartz are shown in Fig. 8b. At high-T conditions above 800 °C, recrystallized grain size shows only a weak dependence on temperature. This result is consistent with the conclusion of Stipp and Tullis (2003), who detected no remarkable temperature effects within the stress resolution of the Griggs-type apparatus; however, at low-T metamorphic conditions, the temperature dependence of grain size becomes significant. For example, at 1000 °C in the β-quartz stability field, a recrystallized grain size of 50 μm gives a flow stress of about 27 MPa, whereas at 400 °C in the α-quartz field the stress is estimated to be about 56 MPa. For a grain size of 20 μm, we obtain a flow stress of about 55 MPa at 1000 °C and a stress in excess of 110 MPa at 400 °C. If the empirical d–σ relations obtained at high temperatures are directly applied to natural rocks deformed under low-temperature metamorphic conditions, the errors in stress estimates may exceed 50 MPa for fine-grained rocks. The strength of the crust would be considerably underestimated if the temperature effects in piezometric relations are neglected.

The temperature dependence of the d–σ relation is not detected in quartz and olivine (Drury, 2005) but is clearly shown in a Mg-alloy (De Bresser et al., 1998; $\Delta Q/m = -29.3 \pm 4.0$ kJ/mol) and halite (Ter Heege et al., 2005a; $\Delta Q/m = -7.7 \pm 2.1$ kJ/mol for the median grain size). Ter Heege et al. (2005a) noted that the apparent activation energy $\Delta Q/m$ quantified in their experiment is inconsistent with the Shimizu model when $Q_v = 205$–221 kJ/mol obtained by direct diffusion measurements and $Q_{gb} = 24.5$ kJ/mol of pressure solution creep are applied to Eq. (21). The process that actually controls the climb velocity in halite is inferred to be faster than volume diffusion, because $Q_c = 51.6$ kJ/mol of the low-stress flow law of Carter et al. (1993) (assigned as climb-controlled creep) and $Q_c = 68.1$ kJ/mol of the high-stress flow law (assigned as cross-slip controlled creep) are much smaller than Q_v. The inconsistency between Q_c and the measured value of Q_v is not presently satisfactorily explained (Ter Heege et al., 2005b). If the rate-controlling process of subgrain formation is the same as that of 'climb-controlled creep' of Carter et al. (1993), Q_c of the low-stress flow law should appear instead Q_v in Eq. (21), after some modifications to the nucleation model in the Shimizu theory. In this case, $\Delta Q/m$ is evaluated to be −6.8 kJ/mol for the case of intracrystalline nucleation, which shows fair agreement with the empirical value.

7. Conclusions

(1) Different types of DRX are classified based on the type of nucleation mechanism, occurrence of GBM, and time-evolution of recrystallization microstructures. Continuous DRX with SGR nucleation is common in minerals under relatively high-T/low-$\dot{\varepsilon}$ conditions, whereas discontinuous DRX with BLG nucleation takes place under low-T/high-$\dot{\varepsilon}$ conditions.

(2) The relations between DRX mechanisms and theoretical models of recrystallized grain size are summarized in Table 1. Although the theory presented by Twiss (1977, 1980) is meaningful for subgrain size, its applicability to recrystallized grain size is questionable. Physically meaningful theories for the development of steady-state grain size all predict a weak temperature dependence in the following form:

$$\frac{d}{b} = B\left(\frac{\sigma}{\mu}\right)^{-p} \exp\left(-\frac{\Delta Q}{mRT}\right).$$

(3) Laboratory data obtained for minerals and metals indicate a weak correlation between the stress exponent p of recrystallized grain size and n of dislocation creep flow laws. The exponent p of minerals resulting from SGR + GBM recrystallization is well explained by the theory of Shimizu (1998b), and in some cases is compatible with the field boundary model.

(4) The grain size piezometer for quartz is calibrated in Eqs. (28) and (30) using the intracrystalline SGR + GBM model. The theoretical equation for β-quartz is in good agreement with the experimental results of Stipp and Tullis (2003). The temperature dependence of grain size cannot be ignored in paleostress estimates. If piezometric relations obtained from high-temperature (~1000 °C) experiments are directly apply to fine-grained metamorphic rocks deformed under low-temperature conditions (≤400 °C), the errors in stress estimates may exceed 50 MPa.

Acknowledgements

I am grateful to J. Ter Heege and M. Stipp for thorough reviews that led to improvements in the manuscript. I would also like to thank C.J. Spiers and J.H.P. De Bresser for valuable discussions and H. Nagahama and M. Takahashi for kindly providing a copy of Twiss's (1980) paper. This work was supported by a Science Research Grant (16340150 and 19340137) from the Japan Society for the Promotion of Science.

Appendix

A. Driving force of GBM

In materials deformed by dislocation creep, the main driving force of GBM is the difference in strain energy across a grain boundary. Consider a strain-free nucleus in a deformed matrix, where a steady-state value of E_{strain} is achieved. The driving force for growth of the nucleus by GBM is

$$F = E_{\mathrm{strain}}, \tag{A.1}$$

where the right-hand side is the sum of free dislocation energy E_{disl} and the sub-boundary energy E_{sub}:

$$E_{\mathrm{strain}} = E_{\mathrm{disl}} + E_{\mathrm{sub}} \tag{A.2}$$

The free dislocation energy per unit volume of a material is expressed as

$$E_{\mathrm{disl}} = \rho\zeta \tag{A.3}$$

where ρ is dislocation density and ζ is the dislocation line tension (i.e., self-energy of dislocation per unit length). The following relation is accepted in the theory of dislocation (Nabarro, 1987, Eq. 11.25; Kohlstedt and Weathers, 1980, Eq. 8):

$$\sigma = \alpha\mu b\rho^{\frac{1}{2}}, \tag{A.4}$$

where $\alpha \sim 1$ is a factor that depends on the configuration of the dislocation arrays. Hence, dislocation density is

$$\rho = \left(\frac{\sigma}{\alpha\mu b}\right)^2. \tag{A.5}$$

The dislocation line tension (including the elastic energy in a cylinder of radius r about the dislocation and the energy of the dislocation core) is given as (Hirth and Lothe, 1982)

$$\zeta = \frac{\mu b^2\chi}{4\pi}\ln\left(\frac{\beta r}{b}\right). \tag{A.6}$$

The parameter χ is 1 for a screw dislocation and $1/(1-\nu)$ for an edge dislocation, where ν is Poisson's ratio. For a first-order approximation, it is assumed that all dislocations are edge dislocations; consequently, the expression $\chi = 1/(1-\nu)$ is used hereafter. The constant β is typically 3–4. Considering that the elastic field around a dislocation is cancelled out by other dislocations at the half distance between them, r is given by

$$r = \frac{1}{2}\rho^{-\frac{1}{2}}. \tag{A.7}$$

The substitution of Eqs. (A.5) and (A.7) into Eq. (A.6) yields

$$\zeta = \frac{\mu b^2}{4\pi(1-\nu)}\ln\left(\frac{\beta\alpha\mu}{2\sigma}\right). \tag{A.8}$$

To evaluate the sub-boundary energy, spherical subgrains are considered with diameter d'. The area of a subgrain is $\pi d'^2$, and the number of subgrains occupying a unit volume is

$$N = \frac{6}{\pi d'^3}. \tag{A.9}$$

The area of sub-boundary per unit volume is therefore given by

$$N\pi d'^2\cdot\frac{1}{2} = \frac{3}{d'}. \tag{A.10}$$

The factor 1/2 is included on the left-hand side because the area of each subgrain wall is counted twice. The sub-boundary energy per unit volume of a material is then written as

$$E_{\mathrm{sub}} = \frac{3\gamma}{d'}, \tag{A.11}$$

where γ is the energy per unit area of sub-boundary, given by (Hirth and Lothe, 1982):

$$\gamma = \frac{\mu b^2}{4\pi(1-\nu)h}\xi(\eta). \tag{A.12}$$

Here, h is the mean dislocation spacing, and

$$\xi(\eta) \equiv \eta\coth\eta - \ln(2\sinh\eta) \tag{A.13}$$

$$\eta \equiv \frac{\pi b}{\beta h}. \tag{A.14}$$

Considering a tilt boundary (Fig. 9), h is related to the misorientation angle θ as (Poirier, 1985, Eq. 2.73)

$$\frac{b}{h} = 2\tan\left(\frac{\theta}{2}\right) \simeq \theta. \tag{A.15}$$

The last approximation is justified for low-angle boundaries. Then, Eq. (A.14) becomes

$$\eta = \frac{\pi}{\beta}\theta \ll 1. \tag{A.16}$$

Hence, the following approximations can be applied to Eq. (A.13):

$$\coth\eta \simeq \frac{1}{\eta},\quad \sinh\eta \simeq \eta. \tag{A.17}$$

Eq. (A.12) is then written in terms of θ as

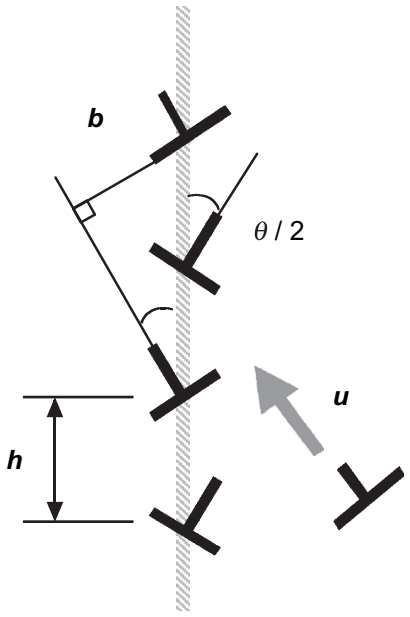

Fig. 9. Schematic illustration of a tilt boundary and a free dislocation climbing toward the boundary at a velocity of u. The misorientation angle θ is exaggerated in this figure.

$$\gamma = \frac{\lambda}{2}\mu b\theta, \tag{A.18}$$

$$\lambda \equiv \frac{1}{2\pi(1-\nu)}\left[1 - \ln\left(\frac{2\pi\theta}{\beta}\right)\right]. \tag{A.19}$$

The substitution of Eqs. (A.5) and (A.8) into Eq. (A.3) yields

$$E_{\mathrm{disl}} = \frac{\sigma^2}{4\pi\alpha^2\mu(1-\nu)}\ln\left(\frac{\beta\alpha\mu}{2\sigma}\right). \tag{A.20}$$

Substituting Eqs. (A.18) and (A.19) into Eq. (A.11) and using Eq. (2) with $p' = 1$, we have

$$E_{\mathrm{sub}} = \frac{3\lambda\theta\sigma}{2K'}. \tag{A.21}$$

From Eqs. (A.2), (A.20), and (A.21), F is scaled as Eq. (3).

B. Twiss's (1980) theory of subgrain size

Here, the scaling relation of subgrain size in Eq. (2) is derived based on the theory presented by Twiss (1980). Let us consider free dislocations with a dislocation density ρ in the initial state. The dislocations are re-arranged into sub-boundaries in the final state. From Eq. (A.10), the area of sub-boundary is $3/d'$ per unit volume. Conservation of the total dislocation length during subgrain formation requires

$$\rho = \frac{3}{d'}\frac{1}{h}. \tag{B.1}$$

The right-hand side represents the length of dislocations contained in sub-boundaries. (Twiss, 1980 only counted dislocations that entered the boundary from one side; hence, his equation (Twiss, 1980, Eq. (10)) differs from Eq. (B.1) by a factor of 2.) Using a low-angle approximation of Eq. (A.15), the above equation is rewritten as

$$\rho = \frac{3\theta}{d'b}. \tag{B.2}$$

A subgrain is stable if the total energy of the sub-boundary becomes smaller than that of the free dislocations; that is,

$$E_{\mathrm{disl}} \geq E_{\mathrm{sub}} \tag{B.3}$$

The equality represents the critical state for the initiation of subgrain formation. With Eqs. (A.3) and (A.11), this condition is written as

$$\rho\zeta \geq \frac{3\gamma}{d'}. \tag{B.4}$$

The right-hand side differs from Eq. (2) of Twiss (1980) (which is identical to Eq. (1) of Twiss, 1977) by a factor of 2.

Eq. (B.4) is now expressed in terms of stress σ. Equating Eqs. (B.2) and (A.5), we have

$$\left(\frac{\sigma}{\alpha\mu b}\right)^2 = \frac{3\theta}{d'b}. \tag{B.5}$$

The substitution of Eqs. (A.5), (A.6), (A.18), and (A.19) into ρ, ζ, and γ of Eq. (B.4) gives

$$\left(\frac{\sigma}{\alpha\mu b}\right)^2 b\ln\left(\frac{\beta\alpha\mu}{2\sigma}\right) \geq \frac{3}{d'}\theta\left[1 - \ln\left(\frac{2\pi\theta}{\beta}\right)\right]. \tag{B.6}$$

Combining Eqs. (B.5) and (B.6), we obtain

$$\ln\left(\frac{\beta\alpha\mu}{2\sigma}\right) \geq \left[1 - \ln\left(\frac{2\pi\theta}{\beta}\right)\right]. \tag{B.7}$$

The condition for a stable misorientation angle is then derived as

$$\theta \geq \frac{e}{\pi\alpha}\left(\frac{\sigma}{\mu}\right), \tag{B.8}$$

where e is the Napierian base.

The initial misorientation angle θ_i at the beginning of subgrain formation is given by the lower limit of Eq. (B.8):

$$\theta_i = \frac{e}{\pi\alpha}\left(\frac{\sigma}{\mu}\right). \tag{B.9}$$

Eq. (20) of Twiss (1980) reduces to the above equation at the limit of a small angle. Because $\mu \geq 10^4$ MPa for minerals, θ_i is usually less than 1°. Applying θ_i of Eq. (B.9) to θ of Eq. (B.5), the initial subgrain size d'_i is obtained as

$$\frac{d'_i}{b} = \frac{3e\alpha}{\pi}\left(\frac{\sigma}{\mu}\right)^{-1}. \tag{B.10}$$

Once the subgrain boundary is established, it acts as a dislocation sink because the total energy is reduced by the arrival of free dislocations into the sub-boundary, which in turn results in a decrease in dislocation spacing h and increase in misorientation angle θ. Progressive subgrain misorientation is therefore an energetically favorable process. Considering that subgrain size is maintained during subsequent misorientation and substituting

$$d' = d'_{\mathrm{i}} \tag{B.11}$$

into Eq. (B.10), we obtain Eq. (2) with $p' = 1$ and

$$K' = \frac{3e\alpha}{\pi}. \tag{B.12}$$

Eq. (14) of Twiss (1980) (identical to Eq. (4) of Twiss, 1977) reduces to a similar form with a slightly different factor.

C. Rate of SGR nucleation

Let us define the nucleation rate I by the number density of nuclei produced in a unit time. Assuming that the nuclei are the same size as the original subgrains, the number of potential nucleation sites per unit volume of crystals is given by Eq. (A.9) for intracrystalline nucleation, and

$$N = \frac{6}{\pi d d'^2} \tag{C.1}$$

for nucleation at grain margins in steady states. The following scaling relation holds:

$$I = \frac{N}{\tau_{\mathrm{c}}}, \tag{C.2}$$

where τ_{c} is the time scale of a nucleation cycle.

During dynamic recovery, sub-boundaries act as a sink of dislocations (see Appendix B). The flux of dislocations that move toward the sub-boundary is given by ρu, where u is the climb velocity (Fig. 9). During one cycle of nucleation events, dislocations are accumulated at the sub-boundary and the misorientation angle reaches a critical value. The time required for dislocations to accumulate in the sub-boundary is equal to the cyclic time τ_{c} of nucleation. It is considered that the subgrain becomes a nucleus when the misorientation angle θ exceeds θ_{c}. From Eq. (A.15), a critical nucleus has a dislocation spacing of $h_{\mathrm{c}} = b/\theta_{\mathrm{c}}$; hence, the

number of dislocations is $1/h_c = \theta_c/b$ per unit area of the boundary. Dividing this value by the flux ρu, the cyclic time is evaluated as

$$\tau_c \simeq \frac{\theta_c}{b\rho u}. \tag{C.3}$$

The climb velocity of dislocations is given by the following (Hirth and Lothe, 1982, Eq. (15)–(90)):

$$u = \frac{\sigma \Omega D_v}{lkT}, \tag{C.4}$$

$$l \equiv \frac{b}{2\pi} \ln\left(\frac{r}{b}\right). \tag{C.5}$$

Here, Ω is the atomic volume and r is the characteristic radius of the elastic field around a dislocation.

Substituting Eqs. (C.3) and (C.4) into Eq. (C.2), using Eqs. (A.9) and (2) with $p' = 1$, and approximating Ω as b^3, we obtain

$$I = \frac{6b^2}{\pi K'^3 \alpha^2 \theta_c} \frac{\sigma D_v}{lkT} \left(\frac{\sigma}{\mu}\right)^5 \tag{C.6}$$

for intracrystalline nucleation; using Eq. (C.1), we obtain

$$I = \frac{6b^2}{\pi K'^2 \alpha^2 \theta_c d} \frac{\sigma D_v}{lkT} \left(\frac{\sigma}{\mu}\right)^4 \tag{C.7}$$

for nucleation at grain margins.

D. Evaluation of scaling factors

This section evaluates the non-dimensional constant $\tilde{B}$ in the nucleation-and-growth model of Shimizu (1998b, 1999). The growth rate $\dot{R}$ of nuclei is written in the form of Eq. (4), with mobility M given by Eqs. (5)–(6) and driving force F by Eqs. (A.1) and (A.2) and (A.20) and (A.21) in Appendix A. A recovered microstructure is assumed, along with $E_{sub} \gg E_{disl} \simeq 0$ for Eq. (A.1). The SGR nucleation rate I is given in Eqs. (C.6) and (C.7) in Appendix C. Substituting these expressions into Eq. (13), we obtain Eq. (16) with

$$\tilde{B} = a\left(\frac{\pi K'^2 \alpha^2}{4} \frac{\lambda \theta \theta_c l}{b}\right)^{1/4} \tag{D.1}$$

for intracrystalline nucleation and

$$\tilde{B} = \left(\frac{a^4 \pi K' \alpha^2}{4} \frac{\lambda \theta \theta_c l}{b}\right)^{1/3} \tag{D.2}$$

for grain boundary nucleation. In a previous paper (Shimizu, 1998b), λ in the right-hand side of Eqs. (D.1) and (D.2) was approximated to be unity. A value of $a = 1.12$ for 2D distributions is used to enable comparisons with grain size data measured in thin section. The materials constant α occupies the ranges 0.4–2.6 for metals, 0.5–1 for ionic salts (Takeuchi and Argon, 1976), and 1.34 for calcite (De Bresser, 1996). The experimental data for olivine and quartz fit to a slightly larger value of $\alpha = 3$ (Kohlstedt and Weathers, 1980).

The non-dimensional constant K' is theoretically given by Eq. (B.12), which yields $K' = 2.60$ for $\alpha = 1$ and $K' = 7.8$ for $\alpha = 3$. Experimentally determined values of K' are about 5–13 for pure metals and 7–18 for steel (Takeuchi and Argon, 1976). Twiss (1977) gives $\log K'(1-\nu) = 0.91$ for metals, which yields $K' = 11.6$ for a Poisson's ratio of $\nu = 0.3$. Somewhat larger values ($K' = 25$–35) are reported for halite (Takeuchi and Argon, 1976; Carter et al., 1993). The values of p' and K' reported for olivine show a large degree of scatter (e.g., $p' = 0.67$ and $K' = 212$; Karato et al. (1980)). The empirical values of K' appear to be systematically larger than the theoretical values. The reason for this discrepancy is not clear, but possible explanations include the difficulties involved in identifying subgrains and measuring subgrain size under the optical microscope, and the hierarchy of dislocation substructures (White, 1979a; Schmid et al., 1980; Poirier, 1985). Whereas theoretical equations describe a primary structure, optically visible subgrains may correspond to higher-order structures.

To calculate the steady-state grain size of quartz, the theoretical expression of K' in Eq. (B.12) is tentatively employed, although this may lead to underestimates of subgrain size and recrystallized grain size. The mean misorientation angle of subgrains is taken to be $\theta = 2°$, as obtained for halite using the electron backscatter diffraction (EBSD) technique (Pennock et al., 2005). A value of $\theta_c = 12°$ is used for the critical misorientation angle between low- and high-angle boundaries. The length scale l is about the same order as that of b. Using Eqs. (A.5) and (A.7), Eq. (C.5) becomes

$$l = \frac{b}{2\pi} \ln\left(\frac{\alpha\mu}{2\sigma}\right). \tag{D.3}$$

The right-hand side is weakly dependent on stress. A stress level of 50 MPa was selected for the present estimation. Applying the α and μ values of quartz listed in Table 3, $\tilde{B}$ is evaluated to be 0.84 for the intracrystalline nucleation model and 0.40 for the marginal nucleation model.

E. Scaling model of Austin and Evans (2007)

Austin and Evans (2007) assumed that the rate of grain boundary production is proportional to the rate of mechanical work done on a material by dislocation creep at steady states, and expressed the change in surface energy as

$$\dot{E}_{surf} = \Lambda \sigma \dot{\varepsilon}_{disl}, \tag{E.1}$$

where Λ ($0 < \Lambda < 1$) represents a fraction of energy conserved in the material as surface energy, and a dot denotes a time derivative. Grain size reduction occurs via the generation of new grain boundaries. Using surface tension (or grain boundary energy per unit area) Γ, the surface energy per unit volume is written in a form similar to that of Eq. (A.11):

$$E_{surf} = \frac{3\Gamma}{d}. \tag{E.2}$$

Differentiating the above with respect to time, $\dot{E}_{surf}$ is also written as

$$\dot{E}_{surf} = -\frac{3\Gamma}{d^2} \dot{d}_{red}, \tag{E.3}$$

where $\dot{d}_{red} (< 0)$ represents the rate of grain size reduction arising from the formation of a new grain boundary.

For grain growth, Austin and Evans (2007) used a kinetic law of static grain growth (e.g., Humphreys and Hatherly, 1995) given by the following equations:

$$d^s - d_i^s = Ct, \tag{E.4}$$

$$C = C_0 \exp\left(-\frac{Q_{gb}}{RT}\right), \tag{E.5}$$

where t is time, C_0 is a constant, and the grain growth exponent s is typically 2 for normal grain growth in a single-phase material. The authors defined the rate of grain growth $\dot{d}_{gr}$ in terms of the time derivative of Eq. (E.4):

$$\dot{d}_{gr} = \frac{C_0}{s d^{s-1}} \exp\left(-\frac{Q_{gb}}{RT}\right). \tag{E.6}$$

At steady states, the net change in grain size is zero:

$$\dot{d}_{gr} + \dot{d}_{red} = 0. \tag{E.7}$$

Equating Eqs. (E.1) and (E.3) and combining the result with Eqs. (E.6) and (E.7), the authors obtained

$$d = \left[\frac{3C_0\Gamma}{s\Lambda\sigma\dot{\varepsilon}_{disl}}\exp\left(-\frac{Q_{gb}}{RT}\right)\right]^{\frac{1}{s+1}}, \tag{E.8}$$

which they termed "paleowattmeter". Using Eq. (8) of recovery creep, the above reduces to Eq. (14) with scaling parameters

$$p = \frac{n+1}{s+1},\ m = s+1,\ \Delta Q = Q_{gb} - Q_c \tag{E.9}$$

and

$$B = b\kappa\mu^p,\ \text{where}\ \kappa = \left(\frac{3\Gamma C_0}{\Lambda sA}\right)^{\frac{1}{m}}. \tag{E.10}$$

The basic assumption involved in the Austin–Evans model is that Λ is constant over a wide range of deformation conditions; however, if there exists any dependence of Λ on σ or T, modification of the scaling parameters p, m, and ΔQ is required. Modeling of the elementary processes of grain boundary formation is necessary to derive the exact form of Λ. Austin and Evans (2007) stated that given the material constants of creep and grain growth laws, their model is able to predict recrystallized grain sizes "without fitting"; however, because Eqs. (E8) and (E10) include an unmeasurable parameter Λ, the absolute size of recrystallized grains cannot be determined from their model alone. It appears that the authors assumed an extreme case of no dissipation ($\Lambda = 1$) for their calculations on calcite, quartz, and olivine.

Austin and Evans (2007) argued that piezometric relations of the form of Eq. (1) or (14) contradict the strain localization theory when applied to natural shear zones, whereas their "wattmeter" does not; however, the direct use of theoretical relations would not be valid for protomylonites at the margins of shear zones, because all theoretical models, including their own, assume steady-state creep behaviors and microstructures. Studies of the evolution of grain size from transient to steady states would be required to understand the gradual change in grain size that occurs from the margins of protomylonite zones to the centers of associated ultramylonite zones.

F. Nomenclature

A	Flow law parameter of dislocation creep in Eq. (8) [$Pa^{-n}\,s^{-1}$]
B	Scaling factor of recrystallized grain size in Eq. (14)
$\bar{B}$	Scaling factor of recrystallized grain size in Eq. (16)
C	Scaling factor of normal grain growth in Eq. (E.4) [$m\,s^{-1}$]
C_0	Pre-exponential constant of C [$m\,s^{-1}$]
D	Effective diffusion coefficient in diffusion creep [$m^2\,s^{-1}$]
D_{gb}	Self-diffusion coefficient at a grain boundary [$m^2\,s^{-1}$]
D^0_{gb}	Pre-exponential constant for D_{gb} [$m^2\,s^{-1}$]
D_v	Self-diffusion coefficient in a grain volume [$m^2\,s^{-1}$]
D^0_v	Pre-exponential constant for D_v [$m^2\,s^{-1}$]
E_{disl}	Free dislocation energy per unit volume [$J\,m^{-3}$]
E_{sub}	Sub-boundary energy per unit volume [$J\,m^{-3}$]
E_{strain}	Strain energy per unit volume [$J\,m^{-3}$]
E_{sur}	Surface energy per unit volume [$J\,m^{-3}$]
F	Driving force of grain growth [$J\,m^{-3}$]
I	Nucleation rate [$m^{-3}\,s^{-1}$]
I_{gb}	Nucleation rate at grain margins [$m^{-3}\,s^{-1}$]
K	Scaling factor in Eq. (1) of recrystallized grain size
K'	Scaling factor in Eq. (2) of subgrain size
L_d	Total length of free dislocations [m]
L	Total length of dislocations in sub-boundaries [m]
M	Mobility of a grain boundary [$J^{-1}\,m\,s^{-1}$]
N	Number density of subgrains [m^{-3}]
P_c	Confining pressure [Pa]
Q	Activation energy of dislocation creep [$J\,mol^{-1}$]
Q_{gb}	Activation energy of grain boundary diffusion [$J\,mol^{-1}$]
Q	Activation energy of dissolution [$J\,mol^{-1}$]
Q_v	Activation energy of volume diffusion [$J\,mol^{-1}$]
ΔQ	Scaling parameter of recrystallized grain size in Eq. (14) [$J\,mol^{-1}$]
R	Gas constant = 8.314510 [$J\,mol^{-1}\,K^{-1}$]
$\dot{R}$	Radial growth rate of a recrystallized grain [$m\,s^{-1}$]
T	Temperature [K]
V	Molar volume [$m^3\,mol^{-1}$]
a	Scaling factor of grain size in Eq. (13)
a_{gb}	Scaling factor of grain size in Eq. (12)
b	Length of the Burgers vector [m]
c	Parameter of creep mechanisms defined by Eq. (23)
d	Recrystallized grain size [m]
d'	Subgrain size [m]
$\hat{d}$	Average grain size defined at the mode of logarithmic grain size [m]
d	Initial grain size [m]
d'	Initial subgrain size [m]
e	Napierian base = 2.71828
f	Fugacity [Pa]
h	Spacing of dislocations in a sub-boundary [m]
j	Stress exponent in Eq. (3)
k	Boltzmann constant = 1.380658×10^{-23} [$J\,K^{-1}$]
l	Length scale defined by Eq. (C.5) [m]
m	Scaling parameter in Eq. (14)
n	Stress exponent of dislocation creep in Eq. (8)
p	Stress exponent of recrystallized grain size in Eqs. (1) and (14)
p'	Stress exponent of subgrain size in Eq. (2)
r	Half distance of dislocations [m]
s	Exponent of normal grain growth in Eq. (E.4)
t	Time [s]
u	Velocity of dislocation climb [$m\,s^{-1}$]
w	Grain boundary width [m]
α	Material constant in Eq. (A.4)
β	Factor in Eq. (A.6)
Γ	Energy per unit area of a grain boundary [$J\,m^{-2}$]
γ	Energy per unit area of a sub-boundary [$J\,m^{-2}$]
ε	Strain
$\dot{\varepsilon}$	Strain rate [s^{-1}]
$\dot{\varepsilon}_{disl}$	Strain rate of dislocation creep [s^{-1}]
$\dot{\varepsilon}_{diff}$	Strain rate of diffusion creep [s^{-1}]
ζ	Dislocation line tension [$J\,m^{-1}$]
η	Parameter defined by Eq. (A.14)
θ	Misorientation angle [rad]
θ_c	Critical misorientation angle [rad]
θ_i	Initial misorientation angle [rad]
κ	Scaling factor given by Eq. (E.10)
Λ	Scaling factor in Eq. (E.1)
λ	Factor defined by Eq. (A.19)
μ	Shear modulus [Pa]
ν	Poisson's ratio
ξ	Function defined by Eq. (A.13)
ρ	Dislocation density [m^{-2}]
σ	Differential stress [Pa]
τ_c	Time scale of nucleation cycle [s]
χ	Parameter of dislocations in Eq. (A.6)
Ω	Atomic volume [m^3]

References

Austin, N.J., Evans, B., 2007. Paleowattmeters: A scaling relation for dynamically recrystallized grain size. Geology 35, 343–346.

Avé Lallemant, H.G., 1978. Experimental deformation of diopside and websterite. Tectonophysics 48, 1–27.

Avé Lallemant, H.G., 1985. Subgrain rotation and dynamic recrystallization of olivine, upper mantle diaprism, and extension of Basin-and-Range province. Tectonophysics 119, 89–117.

Bailey, D.W., Hirsch, P.B., 1962. The recrystallization process in some polycrystalline metals. Proceedings of Royal Society A267, 11–30.

Bellier, S.P., Doherty, R.D., 1977. The structure of deformed aluminum and its recrystallization – investigations with transmission Kossel diffraction. Acta Metallurgica 25, 521–538.

Berman, R.G., 1988. Internally-consistent thermodynamic data for minerals in the system Na_2O–K_2O–CaO–MgO–FeO–Fe_2O_3–Al_2O_3–SiO_2–TiO_2–H_2O–CO_2. Journal of Petrology 29, 455–522.

Blaz, L., Sakai, T., Jonas, J.J., 1983. Effect of initial grain size on dynamic recrystallization of copper. Metal Science 17, 609–616.
Burrows, S., Humphreys, J., White, S., 1979. Dynamic recrystallization. A comparison between magnesium and quartz. Bulletin of Minéralogy 102, 75–79.
Carter, N.L., Horseman, S.T., Russel, J.E., Handin, J., 1993. Rheology of rocksalt. Journal of Structural Geology 15, 1257–1271.
Chopra, P.N., Paterson, M.S., 1984. The role of water in the deformation of dunite. Journal of Geophysical Research 89, 7861–7876.
Christie, J.M., Ord, A., 1980. Flow stress from microstructures of mylonites: example and current assessment. Journal of Geophysical Research 85, 6253–6262.
Cox, S.F., Etheridge, M.A., Hobbs, B.E., 1981. The experimental ductile deformation of polycrystalline and single crystal pyrite. Economic Geology 76, 2105–2117.
De Bresser, J.H.P., 1996. Steady state dislocation densities in experimentally deformed calcite materials: single crystals versus polycrystals. Journal of Geophysical Research 101, 22189–22201.
De Bresser, J.H.P., 2002. On the mechanisms of dislocation creep of calcite at high temperature: inferences from experimentally measured pressure sensitivity and strain rate sensitivity of flow stress. Journal of Geophysical Research 107 (B12), 2337, doi:10.1029/2002JB001812.
De Bresser, J.H.P., Peach, C.J., Reijs, J.P.J., Spiers, C.J., 1998. On dynamic recrystallization during solid state flow: effects of stress and temperature. Geophysical Research Letters 25, 3457–3460.
De Bresser, J.H.P., Ter Heege, J.H., Spiers, C.J., 2001. Grain size reduction by dynamic recrystallization: can it result in major rheological weakening? International Journal of Earth Sciences 90, 28–45.
Derby, B., 1990. Dynamic recrystallization and grain size. In: Barber, D.J., Meredith, P. G. (Eds.), Deformation Processes in Minerals, Ceramics and Rocks. Unwin Hyman, London, pp. 354–364.
Derby, B., 1991. The dependence of grain size on stress during dynamic recrystallization. Acta Metallurgica and Materialia 39, 955–962.
Derby, B., Ashby, M.F., 1987. On dynamic recrystallization. Scripta Metallurgica 21, 879–884.
Drury, M.R., 2005. Dynamic recrystallization and strain softening of olivine aggregates in the laboratory and lithosphere. In: Geological Society of London, Special Publications, vol. 243 143–158.
Drury, M.R., Humphreys, F.J., White, S.H., 1985. Large strain deformation studies using polycrystalline magnesium as a rock analogue. II: dynamic recrystallization mechanisms at high temperatures. Physics of Earth and Planetary Interior 40, 208–222.
Drury, M.R., Urai, J.L., 1990. Deformation-related recrystallization processes. Tectonophysics 172, 235–253.
Dunlap, J.W., Hirth, G., Teyssier, C., 1997. Thermomechanical evolution of a ductile duplex. Tectonics 16, 983–1000.
Edward, G.H., Etheridge, M.A., Hobbs, B.E., 1982. On the stress dependence of subgrain size. Textures and Microstructures 5, 127–152.
Etheridge, M.A., Wilkie, J.C., 1981. An assessment of dynamically recrystallized grainsize as a paleopiezometer in quartz-bearing mylonite zones. Tectonophysics 78, 475–508.
Farver, J., Yund, R.A., 1991a. Oxygen diffusion in quartz: dependence on temperature and water fugacity. Chemical Geology 90, 55–70.
Farver, J., Yund, R.A., 1991b. Measurement of oxygen grain boundary diffusion in natural, fine-grained, quartz aggregates. Geochimica et Cosmochimica Acta 55, 1597–1607.
Farver, J., Yund, R.A., 2000. Silicon diffusion in a natural quartz aggregate: constraints on diffusion transfer creep. Tectonophysics 325, 193–205.
Freeman, B., Ferguson, C.C., 1986. Deformation mechanism maps and microtectonics of rock with distributed grain sizes. Journal of Geophysical Research 91, 3849–3860.
Frost, H.J., Ashby, M.F., 1982. Deformation Mechanism Maps. Pergamon Press, Oxford, 166 pp.
Friedman, M., Higgs, N.G., 1981. Calcite fabrics in experimental shear zones. In: Carter, N.L., Friedman, M., Logan, J.M., Strearns, D.W. (Eds.), Mechanical Behavior of Crustal Rocks. Geophysical Monograph 24. American Geophysical Union, pp. 11–27.
Gleason, G.C., Tullis, J., 1995. A flow law for dislocation creep of quartz aggregates determined with the molten salt cell. Tectonophysics 247, 1–23.
Glover, G., Sellars, M., 1973. Recovery and recrystallization during high temperature deformation of α-iron. Metallurgical Transactions 4, 765–774.
Gottstein, G., Mecking, H., 1985. Recrystallization. In: Wenk, H.-R. (Ed.), Preferred Orientation in Deformed Metals and Rocks: An Introduction to Modern Texture Analysis. Academic Press, Orlando, pp. 183–218.
Giletti, B.J., Yund, R.A., 1984. Oxygen diffusion in quartz. Journal of Geophysical Research 89, 4039–4046.
Guillopé, M., Poirier, J.-P., 1979. Dynamic recrystallization during creep of single-crystalline halite: an experimental study. Journal of Geophysical Research 84, 5557–5567.
Hillert, M., 1965. On the theory of normal and abnormal grain growth. Acta Metallurgica 13, 227–238.
Hirth, J.P., Lothe, J., 1982. Theory of Dislocations, second ed. John Wiley & Sons, New York, 857 pp.
Hirth, G., Tullis, J., 1992. Dislocation creep regimes in quartz aggregates. Journal of Structural Geology 14, 145–159.
Hirth, G., Teyssier, C., Dunlap, J.W., 2001. An evaluation of quartzite flow laws based on comparisons between experimentally and naturally deformed rocks. International Journal of Geophysical Research 90, 77–87.
Hobbs, B.E., 1968. Recrystallization of single crystals quartz. Tectonophysics 6, 353–401.
Humphreys, F.J., Hatherly, M., 1995. Recrystallization and Related Annealing Phenomena. Pergamon, Oxford, 497 pp.
Jacka, T.H., Li, J., 1994. The steady-state crystal size of deforming ice. Annals of Glaciology 20, 1–18.
Jung, H., Karato, S., 2001. Effects of water on dynamically recrystallized grain-size in olivine. Journal of Structural Geology 23, 1337–1344.
Karato, S., Paterson, M.S., Fitz Gerald, J.D., 1986. Rheology of synthetic olivine aggregates: influence of grain size and water. Journal of Geophysical Research 91, 8151–8176.
Karato, S., Toriumi, M., Fujii, T., 1980. Dynamic recrystallization of olivine single crystals during high-temperature creep. Geophysical Research Letters 7, 649–652.
Kohlstedt, D.L., Weathers, M.S., 1980. Deformation-induced microstructures, paleopiezometers, and differential stress in deeply eroded fault zones. Journal of Geophysical Research 85, 6269–6285.
Luan, F.C., Paterson, M.S., 1992. Preparation and deformation of synthetic aggregates of quartz. Journal of Geophysical Research 97, 301–320.
Luton, M.J., Sellars, C.M., 1969. Dynamic recrystallization in nickel and nickel-iron alloys during high temperature deformation. Acta Metallurgica 19, 1033–1043.
Masuda, T., 1982. A microstructural sequence of quartz schists in central Shikoku, southwest Japan. Tectonophysics 83, 329–345.
Masuda, T., Fujimura, A., 1981. Microstructural development of fine-grained quartz aggregates by syntectonic recrystallization. Tectonophysics 72, 105–128.
Mercier, J.-C.C., 1980. Magnitude of continental lithospheric stresses inferred from rheomorphic petrology. Journal of Geophysical Research 85, 6293–6303.
Mercier, J.-C.C., Anderson, D.A., Carter, N.L., 1977. Stress in the lithosphere: inferences from steady state flow of rocks. Pure and Applied Geophysics 115, 199–226.
Nabarro, F.R.N., 1987. Theory of Crystal Dislocations. Dover, New York, 821 pp.
Ord, A., Christie, J.M., 1984. Flow stress from microstructures in mylonitic quartzites of the Moine Thrust zone, Assynt area, Scotland. Journal of Structural Geology 6, 639–654.
Parrish, D.K., Krivz, A., Carter, N.L., 1976. Finite element folds of similar geometry. Tectonophysics 32, 183–207.
Passtier, C.W., Trouw, R.A., 2005. Microtectonics, second ed. Springer, Berlin, 366 pp.
Paterson, M.S., 1989. The interaction of water with quartz and its influence in dislocation flow – an overview. In: Karato, S., Toriumi, M. (Eds.), Rheology of solids and of the Earth. Oxford University Press, Oxford, pp. 107–142.
Pennock, G.M., Drury, M.R., Spiers, C.J., 2005. The development of subgrain misorientation with strain in dry synthetic NaCl measured using EBSD. Journal of Structural Geology 27, 2159–2170.
Pieri, M., Burlini, L., Kunze, K., Stretton, I., Olgaard, D.L., 2001. Rheological and microstructural evolution of Carrara marble with high shear strain: results from high temperature torsion experiments. Journal of Structural Geology 23, 1393–1413.
Poirier, J.-P., 1985. Creep of Crystals. Cambridge University Press, Cambridge, 260 pp.
Poirier, J.-P., Nicolas, A., 1975. Deformation-induced recrystallization by progressive misorientation of subgrain-boundaries, with special reference to mantle peridotites. Journal of Geology 83, 707–720.
Post, R.L., 1973. The flow laws of Mt. Burnett dunite, Ph.D. thesis. University of California, Los Angeles, 272pp.
Post, R.L., 1977. High-temperature creep of Mt. Burnett dunite. Tectonophysics 42, 75–110.
Post, A., Tullis, J., 1999. A recrystallized grain size piezometer for experimentally deformed feldspar aggregates. Tectonophysics 303, 159–173.
Renner, J., Evans, B., 2002. Dislocation creep of calcite. Journal of Geophysical Research 107 (B12), 2364, doi:10.1029/2001JB001680.
Renner, J., Evans, B., Siddiqi, G., 2002. Do calcite rocks obey the power-law creep equation? In: De Meer, S., Drury, M.R., De Bresser, J.H.P., Pennock, G.M. (Eds.), Deformation Mechanisms, Rheology and Tectonics: Current Status and Future Perspectives. Geological Society of London, Special Publication, pp. 293–307.
Richardson, G.J., Sellars, C.M., McTegart, W.J., 1966. Recrystallization during creep of nickel. Acta Metallurgica 14, 1225–1236.
Ross, J.V., Avé Lallemant, H.G., Carter, N.L., 1980. Stress dependence of recrystallized-grain and subgrain size in olivine. Tectonophysics 70, 39–61.
Ross, J.V., Nielson, K.C., 1978. High-temperature flow of wet polycrystalline enstatite. Tectonophysics 44, 233–261.
Rutter, E.H., 1995. Experimental study of the influence of stress, temperature, and strain on the dynamic recrystallization of Carrara marble. Journal of Geophysical Research 100, 24651–24663.
Rutter, E.H., Brodie, K.H., 2004a. Experimental grain size-sensitive flow of hot-pressed Brazilian quartz aggregates. Journal of Structural Geology 26, 2011–2023.
Rutter, E.H., Brodie, K.H., 2004b. Experimental intracrystalline plastic flow in hot-pressed synthetic quartzite prepared from Brazilian quartz crystals. Journal of Structural Geology 26, 259–270.
Sah, J.P., Richardson, G.J., Sellars, C.M., 1974. Grain size effects during dynamic recrystallization of nickel. Metal Science 8, 325–331.
Sakai, T., 1989. Dynamic recrystallization of metallic materials. In: Karato, S., Toriumi, M. (Eds.), Rheology of Solids and of the Earth. Oxford University Press, Oxford, pp. 284–307.
Sakai, T., Jonas, J.J., 1984. Dynamic recrystallization: mechanical and microstructural considerations. Acta Metallurgica 32, 189–209.
Schmid, S.M., Paterson, M.S., Boland, J.N., 1980. High temperature flow and dynamic recrystallization in Carrara marble. Tectonophysics 65, 245–280.

Sellars, C.M., 1978. Recrystallization of metals during hot deformation. Philosophical Transactions of Royal Society of London, Series A 288, 147–158.
Shimizu, I., 1995. Kinetics of pressure solution creep in quartz: theoretical considerations. Tectonophysics 245, 121–134.
Shimizu, I., 1998a. Lognormality of crystal size distribution in dynamic recrystallization. Forma 13, 1–11.
Shimizu, I., 1998b. Stress and temperature dependence of recrystallized grain size: a subgrain misorientation model. Geophysical Research Letters 25, 4237–4240.
Shimizu, I., 1999. A stochastic model of grain size distribution during dynamic recrystallization. Philosophical Magazine A79, 1217–1231.
Shimizu, I., 2003. Grain size evolution in dynamic recrystallization. In: Material Science Forum, vols. 426–432. Trans Tech Publications, Switzerland. 3587–3592.
Stipp, M., Kunze, K., 2008. Dynamic recrystallization near the brittle-plastic transition in naturally and experimentally deformed quartz aggregates. Tectonophysics, doi:10.1016/j.tecto.2007.11.041.
Stipp, M., Tullis, J., 2003. The recrystallized grain size piezometer for quartz. Geophysical Research Letters 30, 2088, doi:10.1029/2003GL018444.
Stipp, M., Tullis, J., Behrens, H., 2006. Effect of water on dislocation creep microstructure and flow stress of quartz and implications for the recrystallized grain size piezometer. Journal of Geophysical Research 111, B04201, doi:10.1029/2005JB003852.
Stipp, M., Stünitz, H., Heilbronner, R., Schmid, S.M., 2002a. The eastern Tonale fault zone: a "natural laboratory" for crystal plastic deformation of quartz over a temperature range from 250° to 700 °C. Journal of Structural Geology 24, 1861–1884.
Stipp, M., Stünitz, H., Heilbronner, R., Schmid, S.M., 2002b. Dynamic recrystallization of quartz: correlation between natural and experimental conditions. In: De Meer, D., Drury, M.R., De Bresser, J.H.P., Pennock, G.M. (Eds.), Deformation Mechanisms, Rheology and Tectonics: Current Status and Future Perspectives. Geological Society of London, Special Publication, pp. 170–190.
Stöckhert, B., Brix, M.R., Kleinschrodt, R., Hurford, A.J., Wirth, R., 1999. Thermochronometry and microstructures of quartz – a comparison with experimental flow laws and prediction on the temperature of the brittle-plastic transition. Journal of Structural Geology 21, 351–369.
Takeuchi, S., Argon, A.S., 1976. Steady-state creep of single phase crystalline matter at high temperatures. Journal of Materials Science 11, 1547–1555.
Ter Heege, J.H., De Bresser, J.H.P., Spiers, C.J., 2002. The influence of dynamic recrystallization on the grain size distribution and rheological behavior of Carrara marble deformed in axial compression. In: De Meer, S., Drury, M.R., De Bresser, J.H.P., Pennock, G.M. (Eds.), Deformation Mechanisms, Rheology and Tectonics: Current Status and Future Perspectives. Geological Society of London, Special Publication, vol. 200, pp. 119–136.
Ter Heege, J.H., De Bresser, J.H.P., Spiers, C.J., 2004. Composite flow laws for crystalline materials with log-normally distributed grain size: theory and application to olivine. Journal of Structural Geology 26, 1693–1705.
Ter Heege, J.H., De Bresser, J.H.P., Spiers, C.J., 2005a. Dynamic recrystallization of wet synthetic polycrystalline halite: dependence of grain size distribution on flow stress, temperature and strain. Tectonophysics 396, 35–57.
Ter Heege, J.H., De Bresser, J.H.P., Spiers, C.J., 2005b. Rheological behaviour of synthetic rocksalt: the interplay between water, dynamic recrystallization and deformation mechanisms. Journal of Structural Geology 27, 948–963.
Takahashi, M., Nagahama, H., Masuda, T., Fujimura, A., 1998. Fractal analysis of experimentally recrystallized quartz grains and its possible application as a strain rate meter. Journal of Structural Geology 20, 269–275.
Toriumi, M., 1982. Grain boundary migration in olivine at atmospheric pressure. Physics of Earth and Planetary Interior 30, 26–35.
Tullis, J., Yund, R.A., 1985. Dynamic recrystallization of feldspar: a mechanism for ductile shear zone formation. Geology 13, 238–241.
Tungatt, P.D., Humphreys, F.J., 1981. An in-situ optical investigation of the deformation behavior of sodium nitrate – an analogue for calcite. Tectonophysics 78, 661–675.
Tungatt, P.D., Humphreys, F.J., 1984. The plastic deformation and dynamic recrystallization of polycrystalline sodium nitrate. Acta Metallurgica 32, 1625–1635.
Twiss, R.J., 1977. Theory and applicability of a recrystallized grain size paleopiezometer. Pure and Applied Geophysics 115, 227–244.
Twiss, R.J., 1980. Static theory of size variation with stress for subgrains and dynamically recrystallized grains. In: Proceedings of Conference IX: Magnitude of Deviatric Stress in the Earth's Crust and Upper Mantle, vol. II. United States Geological Survey, California, Menlo Park. 665–681.
Twiss, R.J., Sellars, C.M., 1978. Limits of applicability of the recrystallized grain size geopiezometer. Geophysical Research Letters 5, 337–340.
Ulrich, S., Thompson, A.B., Schulmann, K., Casey, M., 2006. Microstructure mechanism map of dynamically recrystallized marble. Tectonophysics 412, 173–182.
Urai, J.L., Means, W.D., Lister, G.S., 1986. Dynamic recrystallization of minerals. In: Geophysical Monograph, vol. 39. American Geophysical Union. 161–199.
van der Wal, D., Chopra, P., Drury, M., Fitz Gerald, J., 1993. Relationships between dynamically recrystallized grain size and deformation conditions in experimentally deformed olivine rocks. Geophysical Research Letters 20, 1479–1482.
White, S.H., 1973. Syntectonic recrystallization and texture development in quartz. Nature 244, 276–278.
White, S.H., 1979a. Difficulties associated with paleostress estimates. Bulletin of Minéralogy 102, 210–215.
White, S.H., 1979b. Grain and sub-grain size variation across a mylonite zone. Contributions to Mineralogy and Petrology 70, 193–202.
Wintsch, R.P., Dunning, J., 1985. The effect of dislocation density on the aqueous solubility of quartz and geologic implications: a theoretical approach. Journal of Geophysical Research 90, 3649–3657.
Yund, R.A., Tullis, J., 1991. Compositional changes of minerals associated with dynamic recrystallization. Contributions to Mineralogy and Petrology 70, 193–202.
Zulauf, G., 2001. Structural style, deformation mechanisms and paleodifferential stress along an exposed crustal section; constraints on the rheology of quartzofeldspathic rocks at supra- and infrastructural levels (Bohemian Massif). Tectonophysics 332, 211–237.